WATER RESOURCES RESEARCH, VOL. 45, W11425, doi:10.1029/2009WR007775, 2009

Ecosystem processes at the watershed scale: Extending optimality theory from plot to catchment

Taehee Hwang,[1] Lawrence Band,[1] and T. C. Hales[2]

Received 26 January 2009; revised 6 August 2009; accepted 20 August 2009; published 21 November 2009.

[1] The adjustment of local vegetation conditions to limiting soil water by either maximizing productivity or minimizing water stress has been an area of central interest in ecohydrology since Eagleson's classic study. This work has typically been limited to consider one-dimensional exchange and cycling within patches and has not incorporated the effects of lateral redistribution of soil moisture, coupled ecosystem carbon and nitrogen cycling, and vegetation allocation processes along topographic gradients. We extend this theory to the hillslope and catchment scale, with in situ and downslope feedbacks between water, carbon and nutrient cycling within a fully transient, distributed model. We explore whether ecosystem patches linked along hydrologic flow paths as a catena evolve to form an emergent pattern optimized to local climate and topographic conditions. Lateral hydrologic connectivity of a small catchment is calibrated with streamflow data and further tested with measured soil moisture patterns. Then, the spatial gradient of vegetation density within a small catchment estimated with fine-resolution satellite imagery and field measurements is evaluated with simulated vegetation growth patterns from different root depth and allocation strategies as a function of hillslope position. This is also supported by the correspondence of modeled and field measured spatial patterns of root depths and catchment-level aboveground vegetation productivity. We test whether the simulated spatial pattern of vegetation corresponds to measured canopy patterns and an optimal state relative to a set of ecosystem processes, defined as maximizing ecosystem productivity and water use efficiency at the catchment scale. Optimal carbon uptake ranges show effective compromises between multiple resources (water, light, and nutrients), modulated by vegetation allocation dynamics along hillslope gradient.

Citation: Hwang, T., L. Band, and T. C. Hales (2009), Ecosystem processes at the watershed scale: Extending optimality theory from plot to catchment, *Water Resour. Res.*, *45*, W11425, doi:10.1029/2009WR007775.

1. Introduction

[2] Eagleson proposed an elegant optimality hypothesis in water-limited ecosystems [*Eagleson*, 1978a, 1978b, 1978c, 1978d, 1978e, 1978f, 1978g, 1982; *Eagleson and Tellers*, 1982], based on the Darwinian approach that "current vegetation composition is an optimal state for productivity" [*Eagleson*, 2002, p. 314]. In the absence of significant disturbance, natural soil-vegetation systems would coevolve "gradually and synergistically" with changes in soil structure driven by vegetation to achieve an equilibrium state. Eagleson posited that these equilibria are based on three different optimization strategies at different temporal scales. At short time scales with given climate and soil conditions, minimization of soil water stress produces a vegetation canopy in which steady state soil moisture will be maximized to minimize vegetation water stress. This short-term equilibrium hypothesis is usually interpreted as a "growth-stress trade-off" [*Mackay*, 2001; *Kerkhoff et al.*, 2004], which conceptually describes the optimal carbon uptake or biomass productivity represented by canopy density in terms of water use. Maximization of biomass productivity is then assumed to control the long-term joint adjustment of vegetation species and soil over successional and quasi-geological time scales respectively. This hypothesis suggests that optimal canopy density in water-limited ecosystems is to be found between minimum water stress and maximum productivity [*Rodriguez-Iturbe et al.*, 1999a].

[3] Over past three decades, the optimization of vegetation structure at the plot scale has been defined in the ecological and hydrological fields as various terms including hydrologic equilibrium concepts for terrestrial vegetation or vegetation species distribution at local [*Nemani and Running*, 1989], catchment [*Mackay*, 2001; *Caylor et al.*, 2004, 2005] and continental scales [*Arris and Eagleson*, 1994], minimization of global water stress through tree/grass coexistence [*Rodriguez-Iturbe et al.*, 1999a, 1999b], emergent optimal water use properties across different biomes [*Huxman et al.*, 2004; *Emanuel et al.*, 2007], and the evaluation of carbon and water fluxes with a short-term physiological optimality hypothesis [*Hari et al.*, 1999, 2000; *Schymanski et al.*, 2008a; *van der Tol et al.*, 2008a, 2008b]. In most cases, the adjustment of the canopy to maximize productivity relative to water availability and flux has been evaluated with respect to one dimensional (vertical) water and nutrient exchange at

[1]Department of Geography and Institute for the Environment, University of North Carolina at Chapel Hill, Chapel Hill, North Carolina, USA.
[2]School of Earth and Ocean Sciences, Cardiff University, Cardiff, UK.

0043-1397/09/2009WR007775$09.00

the ecosystem patch scale, without incorporating lateral moisture redistribution at the landscape scale.

[4] Ecohydrological feedbacks between vegetation patterns and lateral water redistribution have been reviewed in various studies, including interactions between surface runoff generation and patterned vegetation (e.g., "Tiger bush") in semiarid ecosystems [e.g., *Bromley et al.*, 1997; *Howes and Abrahams*, 2003; *Ludwig et al.*, 2005; *Saco et al.*, 2007] and feedbacks between groundwater hydrology and vegetation especially in riparian ecosystems [e.g., *Camporeale and Ridolfi*, 2006]. Spatial patterns of vegetation are often integrated into hillslope-scale hydrological models to explain the active role of vegetation on local water balance and lateral hydrological processes [e.g., *Famiglietti and Wood*, 1994; *Wigmosta et al.*, 1994; *Chen et al.*, 2005]. *Mackay* [2001] previously evaluated the adjustment of canopy density (leaf area index) to soil moisture and soil nutrients at the hillslope and catchment level, with respect to lateral soil moisture transport.

[5] Determining vertical root profiles and the extent of deep roots has also been a main component of optimality models, as root zone moisture dynamics affects stomatal control on leaf carbon and water exchange, and nitrogen cycling and assimilation [*Mackay and Band*, 1997; *Rodriguez-Iturbe et al.*, 1999a; *Band et al.*, 2001; *Mackay*, 2001; *Porporato et al.*, 2003]. Recent studies of optimal rooting strategies have focused on maximum plant water uptake and transpiration in water-limited ecosystems with analytical solutions [*Laio et al.*, 2006] and numerical approaches [*Collins and Bras*, 2007]. Cost and benefit analysis of deep roots for carbon uptake was also integrated to find the optimal rooting depth strategy at local [*Guswa*, 2008] and global scales [*Kleidon and Heimann*, 1998]. In addition, *Schymanski et al.* [2008b] introduced a model of root water uptake dynamically optimizing root surface area to meet the canopy water demand while minimizing carbon costs related to the root maintenance. However, the above models do not simulate shifts of allocation strategies and nutrient availability with changing rooting depth or profiles. Increased allocation to deep roots can lead to decreased allocation to foliar biomass and shallow roots, resulting in less light and nutrient availability.

[6] We explore general principles that would explain the tendency to evolve optimal ecosystem patterns at the hillslope scale, where ecosystem patches exist as part of a drainage chain, or catena, that share some degree of dependency on productivity and resource use with other patches along flow paths. Optimization has been used to represent a number of different concepts in hydrology and ecology, ranging from maximization of ecosystem functions, to parameter calibrations maximizing model fit to measured runoff. We define optimality here as the maximization of ecosystem functions at the hillslope or catchment scale, such as net primary productivity, evapotranspiration or water use efficiency. We investigate whether these self organizing canopy patterns have the emergent property of maximizing long-term (annual to multiannual) ecosystem net primary productivity, evapotranspiration or water use efficiency at the catchment scale, over and above the optimization at individual patches.

[7] The modeling approach we take is fully transient including short-term hydrologic dynamics, long-term canopy growth, and soil biogeochemical evolution, and does not incorporate short or long-term optimality in the process dynamics. Instead, we use our model to investigate whether hydrological and physiological feedbacks result in the emergent property of catchment scale optimality. The basic concept of this study is that lateral water flux produces important gradients in limiting water and nutrient availability, such as upslope patches condition resource availability downslope. Therefore, in the absence of significant human manipulation, current vegetation density gradients within a hillslope and a catchment can be the result of self-organization between adjacent patches in a catenary sequence of flow paths. *Mackay and Band* [1997] and *Mackay* [2001] used an earlier version of our modeling approach to demonstrate the adjustment of canopy leaf area gradients along hydrologic flow paths with soil water and nutrient conditions in catchments in central Ontario and California.

[8] In this study, the model is parameterized with detailed measurements in the Coweeta Long-term Ecological Research (LTER) site. The spatial gradient of vegetation density within a small catchment, estimated with fine-resolution satellite imagery and field measurements, is evaluated with simulated vegetation growth patterns from different rooting and allocation strategies. The modeling study will simulate net primary productivity (NPP) and evapotranspiration (ET) for the different range of vegetation patterns. The goal of this modeling study is to determine if the observed patterns of vegetation density within a small catchment are from long-term ecohydrologic pattern optimization for carbon uptake (e.g., full system productivity or water use efficiency maximization) at the hillslope scale.

2. Model Overview

[9] This study is based on the use of a process-based ecohydrological model (Regional Hydro-Ecological Simulation System (RHESSys)) [*Band et al.*, 1993, 2001; *Mackay and Band*, 1997; *Tague and Band*, 2004] and detailed measurements in the Coweeta LTER site. RHESSys has been adapted from a set of preexisting models; an ecophysiological model (BIOME-BGC) [*Running and Coughlan*, 1988; *Running and Hunt*, 1993; *Kimball et al.*, 1997; *Thornton et al.*, 2002], a quasi-distributed hydrological model (TOPMODEL) [*Beven and Kirkby*, 1979], a microclimate model (MT-CLIM) [*Running et al.*, 1987], and a soil biogeochemical model ($\text{CENTURY}_{\text{NGAS}}$) [*Parton et al.*, 1996]. We review key model processes below.

2.1. Farquhar Photosynthesis Model

[10] The concept of ecosystem optimality emerged from ecophysiologists [*Cowan and Farquhar*, 1977; *Cowan*, 1982], who developed theories based on principles stating that a maximum amount of carbon is assimilated for a given amount of water loss. Their theory related the stomatal conductance with photosynthesis using a constant water use efficiency concept for short and long-term regulations (referred to as "marginal cost"). The Farquhar photosynthesis model [*Farquhar et al.*, 1980] hypothesizes that plants optimize stomatal conductivity dynamically for maximizing carbon uptake with respect to water loss [*Cowan and Farquhar*, 1977; *Farquhar et al.*, 2001]. Farquhar's equations for C3 plants are controlled by two rate-determining steps in the photosynthetic reaction; a carboxylation rate (A_v)

and electron transport rate (A_j), the minimum of which is the net rate of leaf photosynthesis (A) [*Farquhar et al.*, 1980; *de Pury and Farquhar*, 1997]:

$$A = \min\{A_v, A_j\} - R_d \quad (1)$$

where R_d is daily leaf respiration. In the model, R_d is calculated using reference values at 20°C and an empirical relationship between leaf nitrogen content and respiration rate [*Ryan*, 1991]. Carboxylation limited photosynthesis (A_v) is mediated by Rubisco enzyme, and is referred to as Rubisco-limited photosynthesis [*Farquhar et al.*, 1980; *de Pury and Farquhar*, 1997; *Farquhar and von Caemmerer*, 1982]:

$$A_v = V_{\max}\frac{C_i - \Gamma_*}{C_i + K_c(1 + O_i/K_o)} \quad (2)$$

where K_c and K_o are the Michaelis-Menten constant of Rubisco for CO_2 and O_2, and C_i and O_i are partial pressure of within leaf CO_2 and O_2, and Γ_* is the CO_2 compensation point. Both K and Γ_* are temperature-dependent usually expressed with reference values at 25°C and their increase ratios with 10°C increase (Q_{10} values) [*Collatz et al.*, 1991]. $V_{\max}$ represents the maximum rate of carboxylation, assumed to be a linear relationship with leaf nitrogen content per unit leaf area and Rubisco activity, which includes a temperature-dependent function [*de Pury and Farquhar*, 1997; *Chen et al.*, 1999; *Wilson et al.*, 2000].

[11] Electron transport limited photosynthesis (A_j) is catalyzed by Ribulose-bisphosphate carboxylase-oxygenase (RuBP) enzyme, often called RuBP-limited photosynthesis [*Farquhar et al.*, 1980; *Farquhar and von Caemmerer*, 1982; *de Pury and Farquhar*, 1997]:

$$A_j = J\frac{C_i - \Gamma_*}{4.5C_i + 10.5\Gamma_*} \quad (3)$$

where J is the electron transport rate, calculated from a quadratic equation as a function of effective irradiance (I_e) and the maximum electron transport rate ($J_{\max}$). A fixed ratio (2.1; [*Wullschleger*, 1993]) is usually assumed between $J_{\max}$ and $V_{\max}$ even though this ratio can vary with temperature sensitivities of both components.

2.2. Coupled Photosynthesis-Stomatal Conductance Models

[12] Many stomatal conductance (g_s) models [e.g., *Baldocchi et al.*, 1991; *McMurtrie et al.*, 1992; *Sellers et al.*, 1992; *Leuning*, 1995; *Chen et al.*, 1999; *Oren and Pataki*, 2001; *Kim et al.*, 2008] use an empirical equation from *Jarvis* [1976], which assumes that environmental factors act independently to control stomatal conductance:

$$g_s = g_{s.\max} f(VPD) f(\psi) f(APAR) f(CO_2) \quad (4)$$

where $g_{s.\max}$ is the maximum stomatal conductance for water, $f(\cdot)$ are linear or nonlinear scalar functions that evaluate between 0 and 1 for VPD (vapor pressure deficit), ψ (soil water potential), $APAR$ (absorbed photosynthetically active radiation per unit leaf area), and CO_2 (atmospheric concentration of carbon dioxide).

[13] Stomatal conductance is the key link between carbon uptake and water leakage because gas exchange though stomata is usually assumed to be dominated by a diffusion process following concentration gradients under a steady state assumption [*Cowan and Farquhar*, 1977]. Stomatal conductivity for CO_2 (g_c) can be calculated by dividing the above g_s with a constant factor (set to 1.6 [*Cowan and Farquhar*, 1977]) which accounts for the ratio of atmospheric diffusivities between water vapor and CO_2 [*Leuning*, 1995]. The rate of CO_2 transport across stomata (A) can be expressed as a function of stomatal conductivity for carbon (g_c) and a concentration gradient term ($C_a - C_i$) [*Cowan and Farquhar*, 1977]:

$$A = g_c(C_a - C_i) \quad (5)$$

A_v from equation (2) and A_j from equation (3) can be solved using the quadratic equation, by substituting C_i from the above equation [*Farquhar and von Caemmerer*, 1982; *Chen et al.*, 1999]. Note that stomatal conductance and photosynthesis are all unit leaf area basis, not unit ground area basis, which would be scaled up with dynamic separation between sunlit and shaded leaves.

2.3. Scaling Up Fluxes From Leaves to Canopy

[14] Many coupled modeling efforts show that dynamic separation between sunlit and shaded leaves is the most efficient way to represent different rate determining factors for photosynthesis with canopy depth profile without multilayer simulations [*de Pury and Farquhar*, 1997; *Chen et al.*, 1999; *Wang and Leuning*, 1998]. Following *Chen et al.* [1999], total sunlit leaf area index (LAI) (LAI_{sunlit}) is defined as

$$LAI_{sunlit} = 2\cos\theta(1 - \exp(-0.5\Omega LAI/\cos\theta)) \quad (6)$$

where θ is sun zenith angle, and Ω is the foliage clumping index. Shaded LAI (LAI_{shade}) is $LAI_{shade} = LAI - LAI_{sunlit}$. Dynamic weighting is applied to calculate canopy-scale stomatal conductance (g_s), and photosynthesis (A) per unit ground area:

$$g_s = g_{s.sunlit}LAI_{sunlit} + g_{s.shade}LAI_{shade} \quad (7)$$

$$A = A_{sunlit}LAI_{sunlit} + A_{shade}LAI_{shade} \quad (8)$$

[15] This dynamic separation between sunlit and shaded leaves is justified in that the upper canopy is usually light saturated whereas the lower canopy responds linearly to irradiance, which should result in a vertical distribution of leaf nitrogen and specific leaf area for their optimal exploitation [*Field*, 1983; *de Pury and Farquhar*, 1997].

2.4. Nitrogen Limitation

[16] Most temperate forests are limited by nutrients, in particular nitrogen [*Vitousek and Howarth*, 1991; *Schimel et al.*, 1997; *Nadelhoffer et al.*, 1999; *Oren et al.*, 2001]. Most ecohydrological catchment models usually incorporate only soil moisture patterns into vegetation dynamics, derived by topographic position, local soil texture, and available rooting depth information without nutrient limitation [*Wigmosta et al.*, 1994; *Rodriguez-Iturbe et al.*, 1999a; *Porporato*

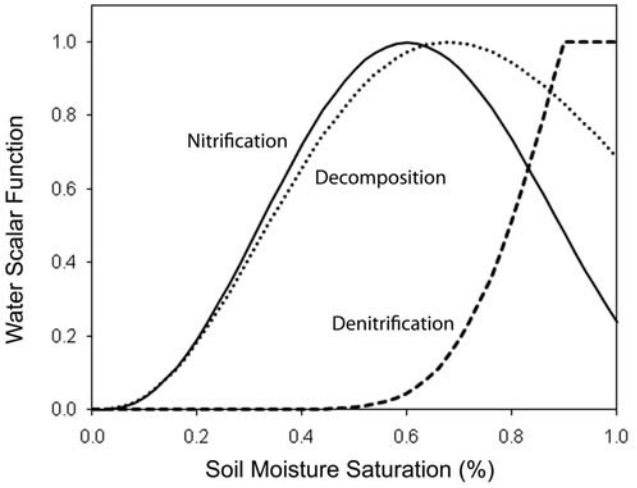

Figure 1. Water scalar functions of nitrogen transformation rates as a function of soil moisture saturation for sandy loam soils [after *Parton et al.*, 1996].

et al., 2002; *Ivanov et al.*, 2008; *van der Tol et al.*, 2008a] and are often applied in strictly water limited ecosystems.

[17] The spatial distribution of plant-available nitrogen is also closely related to local soil moisture dynamics, which itself is a composite result of microclimate condition, local soil texture, and local vegetation; both directly (e.g., mineralization, nitrification, denitrification, and leaching) and indirectly through plants (e.g., translocation, residues decomposition, and nitrogen fixation) [*Mackay and Band*, 1997; *Creed and Band*, 1998a, 1998b; *Band et al.*, 2001; *Mackay*, 2001; *Porporato et al.*, 2003]. Figure 1 shows the adjustment of nitrogen transformation rates as a function of soil moisture content following *Parton et al.* [1996], which determines a direct topographic effect on spatial patterns of plant-available nitrogen. Note that available nitrogen content would be most available around 60% of volumetric soil water saturation for sandy loam soil by increasing anaerobic condition of soil at high soil moisture content, where denitrification process is more active.

[18] The nitrogen cycle in the model is largely based on the BIOME-BGC model [*Running and Coughlan*, 1988; *Running and Hunt*, 1993; *Kimball et al.*, 1997; *Thornton et al.*, 2002] for vegetation and the CENTURY$_{NGAS}$ model [*Parton et al.*, 1996] for soil. The model assumes stoichiometrically constant ratios between carbon and nitrogen (C/N ratio) for all vegetation compartments (leaf, litter, fine root, live wood, and dead wood) and soil pools [*Tague and Band*, 2004]. At a daily time step, all soil/litter pools calculate the potential immobilization and decomposition rates based on soil water and temperature. If nitrogen availability cannot satisfy the sum of potential microbial uptake (immobilization) and plant growth demands (plant uptake), these two demands compete for available soil mineral nitrogen. Plants can also use an internally recycled nitrogen pool translocated from turnover of leaves and live vegetation parts (stem, coarse root) for remaining demands for nitrogen. Available nitrogen also includes atmospheric deposition, fertilization, or symbiotic/asymbiotic fixation. Detailed explanations are available in the works of *Thornton* [1998] and *Tague and Band* [2004].

2.5. Allocation

[19] The amount of fixed carbon available to the leaf depends on subsequent metabolic events after photosynthesis, called allocation, which includes the storage, utilization and transport of fixed carbon in the plant [*Taiz and Zeiger*, 2002]. Interannual effects of climate factors on vegetation are largely from translocation of these stored carbohydrates to leaves in the early growing season [*Taiz and Zeiger*, 2002]. In the model, these allocation dynamics depend on mixed daily and yearly allocation strategies related to temporal phenological changes (Figure 2) [*Running and Hunt*, 1993; *Thornton*, 1998; *Thornton et al.*, 2002]. Daily gross photosynthesis is allocated to both vegetation and storage (available for budburst in the following growing season) at a constant ratio after considering autotrophic respiration (maintenance and growth respirations). Transfer from storage to vegetation compartments occurs during the prescribed growing season. Leaf and fine root turnovers occurs only during the prescribed leaf fall season, whereas those for live stem and coarse root occur at a constant rate throughout the year. Biogeochemical models usually do not simulate actual tree stands which incorporate tree seedling, recruitments, and mortality [*Friend et al.*, 1997]. Only total plant mortality is simulated which describe the portion of the plant pools either replaced each year or removed through fire or plant death.

[20] Note that LAI is not prescribed into the model, but the model is self-regulating with respect to LAI based on photosynthate production, respiration, and allocation processes. Optimality models that prescribe aboveground vegetation density and belowground biomass (or rooting depth)

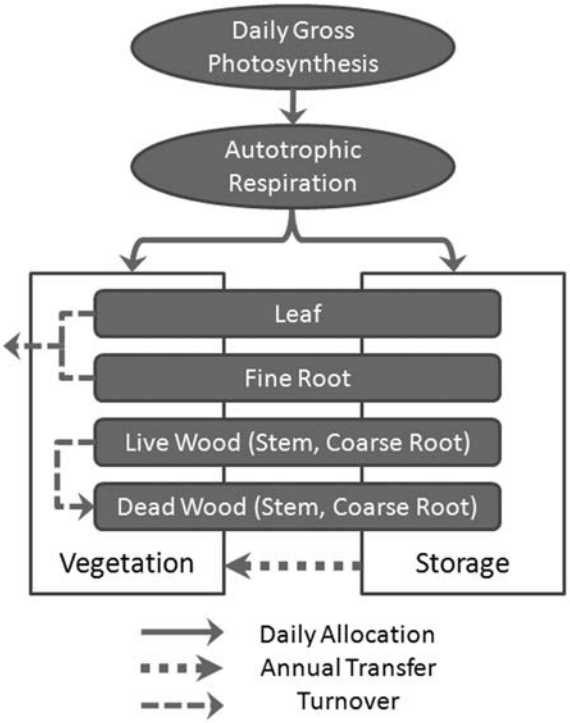

Figure 2. A compartment flow diagram of carbon allocation, transfer, and turnover with mixed daily and yearly allocation strategies following the current BIOME-BGC algorithm [*Thornton*, 1998; *Thornton et al.*, 2002].

usually neglect the feedbacks and constraints of previous, transient carbon, water and nutrient balance. Allocation processes compromise between light, water, and nutrients proportioning fixed carbon into different vegetation compartments based on limiting resources [*Tilman*, 1988; *Gedroc et al.*, 1996; *McConnaughay and Coleman*, 1999].

3. Materials and Methods

3.1. Site Description

[21] The Coweeta Hydrologic Lab (CHL) is located in western North Carolina and is representative of the Southern Appalachian forest. The Southern Appalachian forest has very diverse flora as a result of combined effect of terrain, microclimate and soil moisture [*Whittaker*, 1956; *Day and Monk*, 1974]. Mean monthly temperature varies from 3.6°C in January to 20.2°C in July. The climate in the Coweeta Basin is classified as marine, humid temperate, and precipitation is relatively even in all seasons; annual precipitation ranges from 1870 mm to 2500 mm with about a 5% increase with 100 m [*Swift et al.*, 1988]. The dominant canopy species are oaks and mixed hardwoods including *Quercus* spp. (oaks), *Carya* spp. (hickory), *Nyssa sylvatica* (black gum), *Liriodendron tulipifera* (yellow poplar), and *Tsuga canadensis* (eastern hemlock), while major evergreen undergrowth species are *Rhododendron maximum* (rhododendron) and *Kalmia latifolia* (mountain laurel) [*Day and Monk*, 1974; *Day et al.*, 1988]. The main study site is Watershed 18 (WS18), a northwest facing, steeply sloping (average 52% slope), 13 ha catchment with an elevation range from 726 to 993 m (Figure 3c). This study site is a control watershed with mixed hardwoods stands undisturbed since 1927. Soil moisture is a primary control on vegetation patterns within WS18, despite the high annual rainfall [*Day and Monk*, 1974; *Day et al.*, 1988].

3.2. Climate Data and Historical Field Measurements

[22] Daily climate (maximum and minimum daily temperature, daily precipitation; CS01/RG06 climate station) and streamflow data (WS18; Coweeta LTER research data ID 3033) are available from 1937, one of the longest hydrological records for forested headwater catchments in the world. For the model simulation, we used universal kriging with elevational trends from 7 points measurements within the Coweeta basin from 1991 to 1995 to develop long-term rainfall isohyets to scale daily precipitation over the terrain.

[23] Three LTER research plots have been established along a topographic gradient at high, mid and low catchment positions (118, xeric; 218, mesic; and 318, intermediate) to study ecohydrologic trends within the study watershed (Figure 3b), where detailed vegetation, soil and various microclimate data are available. Detailed explanations of these gradient plots are available at the Coweeta LTER homepage (http://coweeta.ecology.uga.edu/gradient_physical.html). We use daily volumetric water content data (Coweeta LTER research data ID 1013) collected with 30 cm CS615 sensors (Water Content Reflectometer, Campbell Scientific Inc., Logan, UT, USA) every 15 min from March 1999. At each gradient plot, these TDR sensors are installed at different depths ($0 \sim 30$ and $30 \sim 60$ cm) and at two locations (upper slope and lower slope) within 20×40 m original rectangular plots.

[24] Aboveground net primary productivity (ANPP) was estimated from tree ring increments and litterfall measurements in the early 1970s for the full watershed [*Day and Monk*, 1974, 1977; *Day et al.*, 1988]. Biomass increases were estimated from tree ring increments with locally derived biometric equations for each species [*Day and Monk*, 1974, and references therein]. Recently, *Bolstad et al.* [2001] also estimated ANPP at four circular 0.1 ha plots within the watershed (site number 3, 4, 13, 14) from 2 year litterfall ($1995 \sim 1996$) and 10 year tree ring measurements ($1986 \sim 1995$).

3.3. Hydrologic Gradients of Vegetation Density

[25] Leaf area index (LAI), an important carbon state variable in process-based biogeochemical models, is also a valuable driver in the scaling effort as it is well correlated with normalized difference vegetation index (NDVI) derived from remote sensing images [*Gholz et al.*, 1991; *Nemani et al.*, 1993; *Chen and Cihlar*, 1996; *Fassnacht et al.*, 1997]. The NDVI is a normalized ratio between red and near infrared bands:

$$NDVI = (\rho_{NIR} - \rho_{RED})/(\rho_{NIR} + \rho_{RED}) \quad (9)$$

[26] LAI values were measured at 39 points around the WS18 in early June 2007 using two different methods (Figure 3c), with GPS coordinates measured during the previous leaf-off season (GeoExplorer; Field Data Solutions Inc., Jerome, ID, USA). LAI was measured with an LAI-2000 Plant Canopy Analyzer (LI-COR Inc., Lincoln, NE, USA) using two instruments simultaneously for above and below canopy during overcast sky condition or at dawn or at dusk. Hemispheric images were also taken at the same sites, and analyzed with the Gap Light Analyzer software (Institute of Ecosystem Studies, Millbrook, New York, USA). We also used LAI data estimated from litter biomass and specific leaf area around the Coweeta LTER site (Figure 3c), four of which are located within WS18 [*Bolstad et al.*, 2001]. These litter trap measurements are quite valuable in that optical measurements usually do not show much sensitivity in ranges of high leaf area index [*Pierce and Running*, 1988; *Gower and Norman*, 1991; *Nemani et al.*, 1993; *Fassnacht et al.*, 1997].

[27] Spatial patterns of LAI within the watershed were determined from the site-specific correlation between point-measured LAI and NDVI values from a summer IKONOS Image (June 1, 2003; Figure 3a) with varying average window size of NDVI pixels and masking from outmost rings in a sequence for optical LAI calculation. Optical measurements of vegetation using LAI-2000 in complex terrain can be biased by topographic interference especially in the outer rings. We found the best match between LAI calculations of $0° \sim 23°$ zenith ranges (1 and 2 rings) and NDVI values by a 3×3 averaging window (Figure 3a). Considering average canopy height ($\sim$16 m) within the watershed and 4 m IKONOS pixel size, this match is quite reasonable in terms of their size correspondences.

[28] Most LAI measurements are located along the regression line except for some outliers (Figure 4a), from which we estimated spatial patterns of vegetation density within the target watershed. These outliers are mostly from the sites where thick rhododendron (*R. maximum*) develops in under-

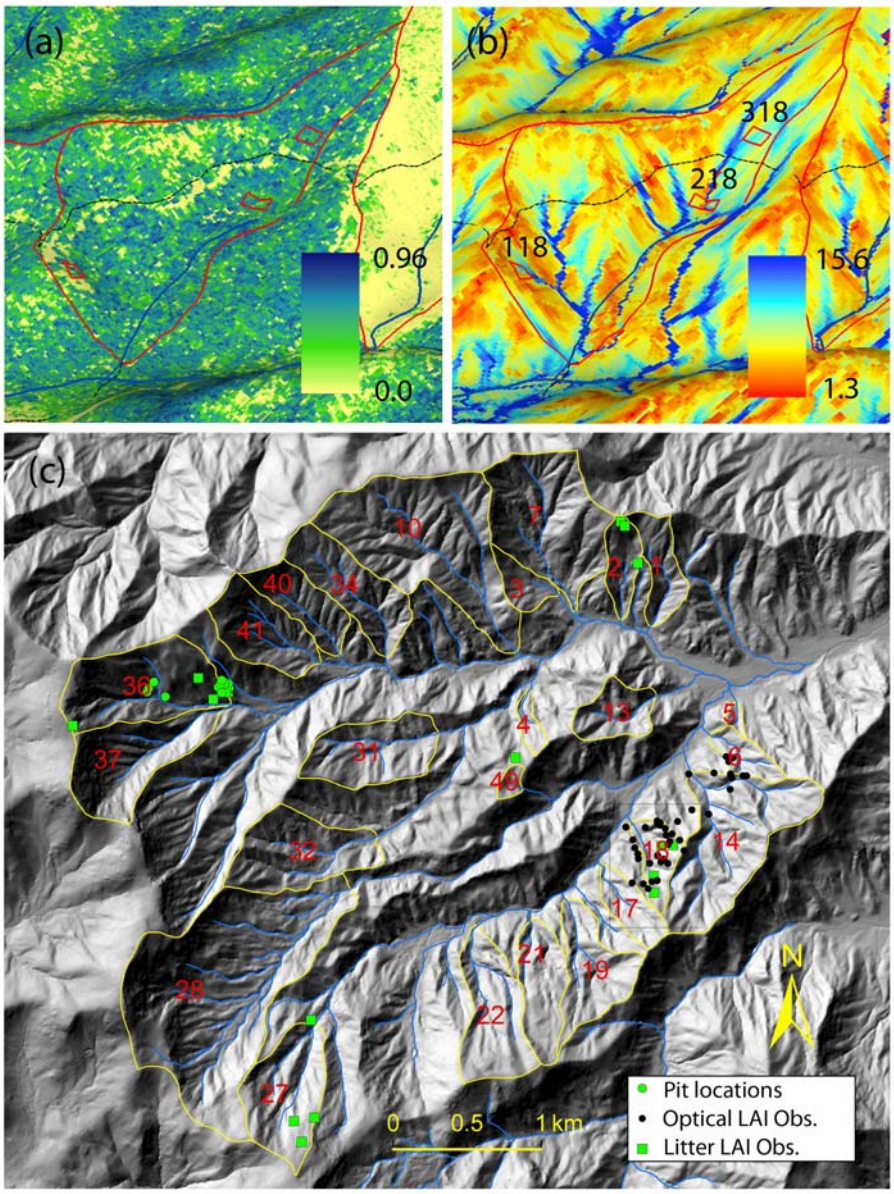

Figure 3. Study site (WS18): (a) normalized difference vegetation index (NDVI) from a June 1, 2003 IKONOS image, (b) wetness index, and (c) locations for WS18 (square), leaf area index (LAI) measurements, and soil pits within the Coweeta LTER site. Red and yellow lines represent the boundaries of watersheds, and dashed lines indicate roads along which artificial gaps are shown. The rectangles within WS18 are three gradient plots (118, 218, and 318). A paired experimental watershed (WS17) is also shown next to the target watershed where white pines (*Pinus strobus* L.) are planted in 1956 after 15 year clear-cut periods.

story canopy. Dense understory canopy can easily decouple upward ground optical measurements and downward remote sensing images, and also affects NDVI values which are very sensitive to canopy background variations [*Huete*, 1988; *Huete et al.*, 1994].

[29] Hydrologic gradients of vegetation density were calculated by grouping 10 × 10 m patches at equal wetness index intervals (0.5) to suppress noises, where only groups over ten pixels were counted (Figure 4b). Wetness index (or topographic index [*Beven and Kirkby*, 1979]) was calculated from 6.1 m (20 ft.) LIDAR elevation data (Figure 3c) representing hydrological gradients in the TOPMODEL algorithm. Upslope contributing area for wetness index was calculated from *D* infinity ($D\infty$) method allowing flow to be proportioned between multiple downslope pixels according to gradient [*Tarboton*, 1997]. A 30 m buffer area along the road is masked in this analysis to exclude artificial vegetation gaps (Figure 3a).

3.4. Rooting Depth and Root Distributions From Soil Pits

[30] *Hales et al.* [2009] estimated spatial distributions of root depth, with 15 manually excavated soil pits around WS36 (Figure 3c), undisturbed since 1919. WS36 has steeper topography (average 65% slope) with steeper gradients of vegetation density (not shown here) than the study watershed

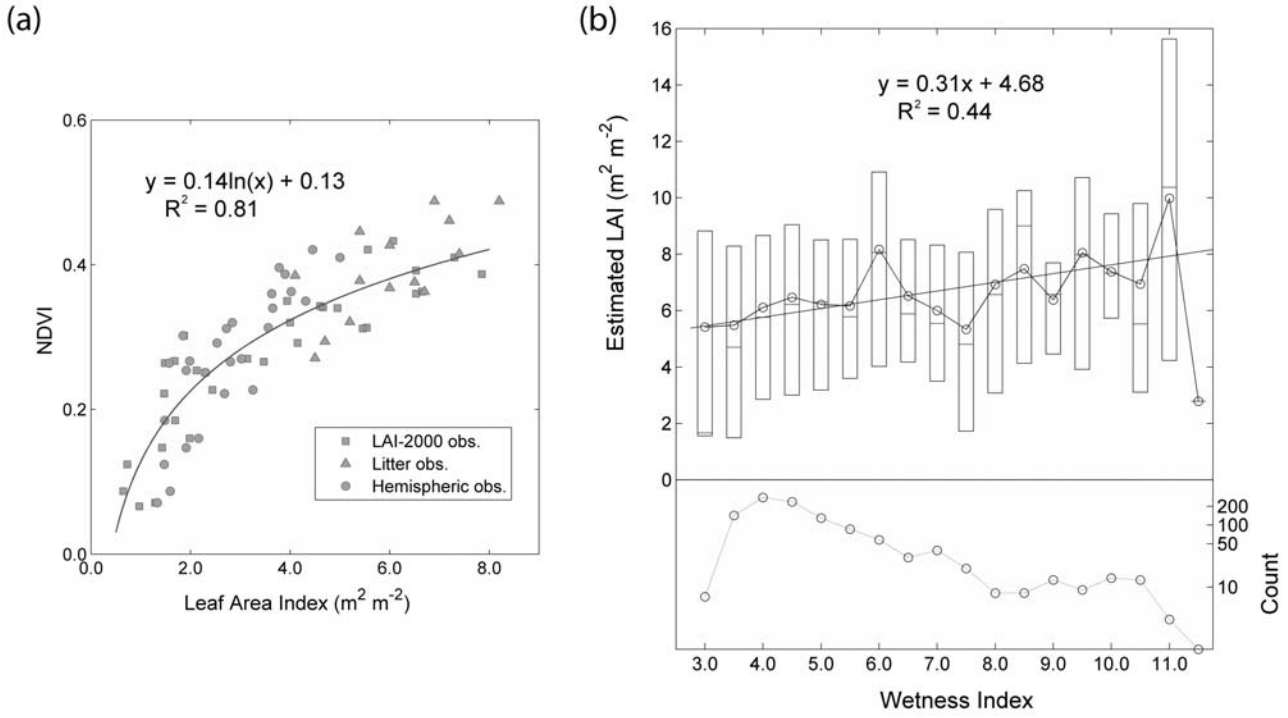

Figure 4. (a) A scatterplot between LAI (leaf area index) measurements and NDVI (normalized difference vegetation index), and (b) hydrologic gradients of estimated LAI within the study watershed. Circles represent average values, and box plots have lines at the lower quartile, median, and upper quartile values from each binned group. Counts are the number of 10 × 10 m patches in each group, which are basic units of model simulation.

(WS18). We did not excavate in WS18 as it is now preserved and adjacent catchments are recently disturbed (e.g., selective logging). Nine pits were located close to the watershed outlet, while another four pits were excavated higher in the watershed (Figure 3c). Soils are all sandy-silt loam inceptisols with a typical colluvial appearance.

[31] Pits were dug with horizontal dimensions of approximately 100 cm by 150 cm, with depth varying between 120 cm and 180 cm due to difficulties excavating pits below the saprolite layer. Each pit was located downslope (within 0.8 m) from an individual specimen of one of the major hardwood species within the Coweeta LTER site (Tables 1 and 2). Pit locations were carefully chosen in the field based on topographic positions, classified based on their curvature as ridge, sideslope, and hollow (Table 1). From GPS coordinates and the LIDAR data, the average wetness index of ridge pits was computed to be 3.79, while that of hollow pits was 5.65. Note that on-site curvature is a more robust method to determine topographic positions for each tree, because even detailed elevation information (e.g., LIDAR) cannot decide a hillslope position of each tree for geolocation or scale problems.

[32] Summaries of soil pit measurements are available in Table 1. Detailed methods of pit construction, root frequency, and diameter measurements are described by *Hales et al.* [2009]. Note that the limited number of measurements was due to careful hand digging to sample fine root structures. The vertical distribution of roots was quantified by counting roots, where the cumulative frequency function of roots was drawn to determine rooting depth and vertical root distribution.

3.5. Model Parameterization

[33] The model is simulated at 10 × 10 m grid cell resolution (patch; n = 1253) which we treat as control volumes for biogeochemical and hydrological processes. Many

Table 1. Detailed Measurements for Soil Pits at Different Topographic Positions

Species	DBH (cm)	Wetness Index	Rooting Depth RD_{95}[a] (m)
	Ridge		
Acer rubrum	5.1	4.12	1.00
Acer saccharum	20.9	3.10	1.01
Carya spp.	38.8	3.97	0.90
Liriodendron tulipifera	20.1	4.08	0.60
Quercus prinus	58.7	2.59	0.93
Quercus rubra	33.2	4.12	1.02
Rhododendron maximum[b]	9.2	4.61	0.98
Tsuga canadensis[b]	33.9	3.70	0.57
Average	27.5	3.79	0.88
	Sideslope		
Liriodendron tulipifera	17.5	3.89	0.74
	Hollow		
Betula lenta	28.5	4.20	0.91
Liriodendron tulipifera	22.5	5.38	0.94
Quercus rubra	84.0	4.60	1.21
Quercus rubra	37.7	7.89	0.71
Quercus velutina	33.7	5.88	0.75
Rhododendron maximum[b]	4.3	5.93	0.92
Average	35.1	5.65	0.91

[a]Defined from 95% cumulative distribution of root counts.
[b]Note that these species are not deciduous broadleaf.

Table 2. Species-Specific Ecophysiologic Model Parameters[a]

Species	Percent Basal Area[b] (%)	Specific Leaf Area (m^2 kg C^{-1})	Shaded to Sunlit SLA Ratio	Leaf CN Ratio	Maximum Leaf Conductance (m s^{-1})	Photosynthetic Parameter	Q_{10} for Autotrophic Respiration	Maximum Rate of Carboxylation (μmol CO_2 m^{-2} s^{-1})
Quercus prinus	21.3	17.8 (22)	2.21 (24)	25.9 (85)		0.0234 (94)	2.33 (31)	14.54 (94)
Acer rubrum	9.3	25.8 (18)	1.78 (22)	18.5 (103)	0.0058 (NA)	0.0167 (221)	2.43 (40)	7.24 (221)
Quercus coccinea	7.9	19.0 (13)	1.39 (18)	18.8 (80)	0.0083 (NA)	0.0133 (84)	2.37 (25)	27.53 (84)
Quercus rubra	6.8	20.8 (15)	1.74 (24)	26.4 (88)		0.0213 (27)	2.42 (27)	12.77 (27)
Liriodendron tulipifera	6.4	26.8 (18)	1.60 (18)	24.2 (85)	0.0110 (NA)	0.0248 (91)	2.24 (29)	10.18 (91)
Carya glabra	5.1	23.8 (20)	1.69 (24)	21.3 (90)		0.0217 (99)	2.46 (36)	9.42 (99)
Kalmia latifolia	5.1	18.9 (NA)		11.5 (NA)	0.0042 (NA)			
Oxydendrum arboreum	4.4	52.4 (10)	1.03 (8)	20.0 (64)			3.02 (14)	
Nyssa sylvatica	3.7					0.0285 (32)		5.62 (32)
Cornus florida	3.2	29.6 (8)	1.78 (9)	21.2 (65)		0.0662 (20)	2.60 (11)	3.40 (20)
Betula lenta	2.7	34.0 (21)	1.68 (21)	25.4 (79)		0.0115 (290)	2.71 (27)	16.95 (290)
Rhododendron maximum	7.4	48.9 (NA)		10.2 (14)	0.0033 (NA)		2.54 (7)	
Weighted average		23.8	1.66	22.1	0.0065	0.0229	2.43	11.37
References[c]	1	2, 3, 4, 5	3	2, 3, 4, 6	4	8	6, 9	8

[a]Detailed explanations of parameters are available in work by *White et al.* [2000]. Numbers in parentheses are sample sizes. NA means not available. SLA is specific leaf area.
[b]All species under 2% (29 species) are not considered.
[c]References are as follows: 1, *Day et al.* [1988]; 2, *Martin et al.* [1998]; 3, *Mitchell et al.* [1999]; 4, *Reich et al.* [1999]; 5, *Bolstad et al.* [2001]; 6, *Vose and Bolstad* [1999]; 7, *Vose and Bolstad* [2007]; 8, *Sullivan et al.* [1996]; 9, *Bolstad et al.* [1999].

species-specific physiological parameters (Table 2) and other (e.g., soil, nutrient) parameters (Table 3) were measured intensively within WS18 and Coweeta LTER site. We calculated representative physiological parameters at the whole catchment scale with these species-specific parameters weighted by vegetation composition within the study watershed (Table 2). We did not simulate the model at the species level, because a detailed vegetation species map is not available and some physiological parameters (e.g., allocation, phenological parameters) are not measured at the species level. Phenological parameters (Table 3) are estimated from 8 day composite Moderate Resolution Imaging Spectroradiometer (MODIS) satellite images for five years ($2001 \sim 2005$), aggregated to the 5×5 km grid scale large enough to include the whole Coweeta basin (21.8 km^2) and minimize geolocation problems.

[34] Lateral hydrologic connectivity within the study watershed is defined by calibrating the model with streamflow data varying the TOPMODEL parameters, m (the decay rate of hydraulic conductivity with depth), and the lateral/vertical K_{sat0} (saturated hydraulic conductivity at surface). Monte Carlo simulation was implemented three thousand times with randomly sampled parameter values within certain acceptable ranges. A 3 year calibration period (October 1999 to September 2002) was chosen to include extreme drought precipitation patterns (Figure 5) for better representations of soil moisture status during drought periods. To allow soil moisture to stabilize, a one and a half year initialization was employed before the calibration period. The Nash-Sutcliffe (N-S) coefficient [*Nash and Sutcliffe*, 1970] for lognormal streamflow discharge was used to evaluate model performance because this objective function is biased toward base flow, closely related to soil moisture status in this study area [*Hewlett*, 1961]. A maximum efficiency value of the calibration period was 0.802, whereas that of a 16 year validation period was 0.873 (Figure 5).

Table 3. Other Model Parameters

Parameters[a]	Value	Units	References[b]
	Ecophysiological Parameters		
CN ratios of leaf litter/fine root/live wood	34.8/51.1/75.6	unitless	1, 2
Q_{10} value for heterotrophic respiration	3.56	unitless	3
Allocation parameters			
Fine root to leaf carbon	1.21	unitless	4, 5, 6
Stem to leaf carbon	1.0	unitless	4, 5, 6
Live wood to total wood carbon	0.16	unitless	7
Coarse root to stem carbon	0.22	unitless	7
Light extinction coefficient k	0.54	unitless	8
Phenological parameters			
Start days of greenup/senescence	105/260	DOY	5 and 5 year MODIS data (2001∼2005)
Length of greenup/senescence period	35/50	days	5 and 5 year MODIS data (2001∼2005)
Whole plant mortality	0.5	%	7, 9, 10
	Soil Texture Parameters		
Sand/clay/silt	55.2/16.9/27.9	%	11, 12, 13
	Nitrogen Input Parameters		
Wet nitrogen deposition rate	0.0010	kg N m^{-2} y^{-1}	14
Biological nitrogen fixation rate	0.0011	kg N m^{-2} y^{-1}	15

[a]Detailed explanations of parameters are available in work by *White et al.* [2000].
[b]References are as follows: 1, *Martin et al.* [1998]; 2, *Vose and Bolstad* [2007]; 3, *Bolstad and Vose* [2005]; 4, *McGinty* [1976]; 5, *Day and Monk* [1977]; 6, *Monk and Day* [1988]; 7, *White et al.* [2000]; 8, *Sullivan et al.* [1996]; 9, *Elliott and Swank* [1994]; 10, *Clinton et al.* [2003]; 11, *Zak et al.* [1994]; 12, *Yeakley et al.* [1998]; 13, unpublished data from T. Lookingbill, 1996–1999; 14, *Knoepp et al.* [2008]; 15, *Todd et al.* [1975].

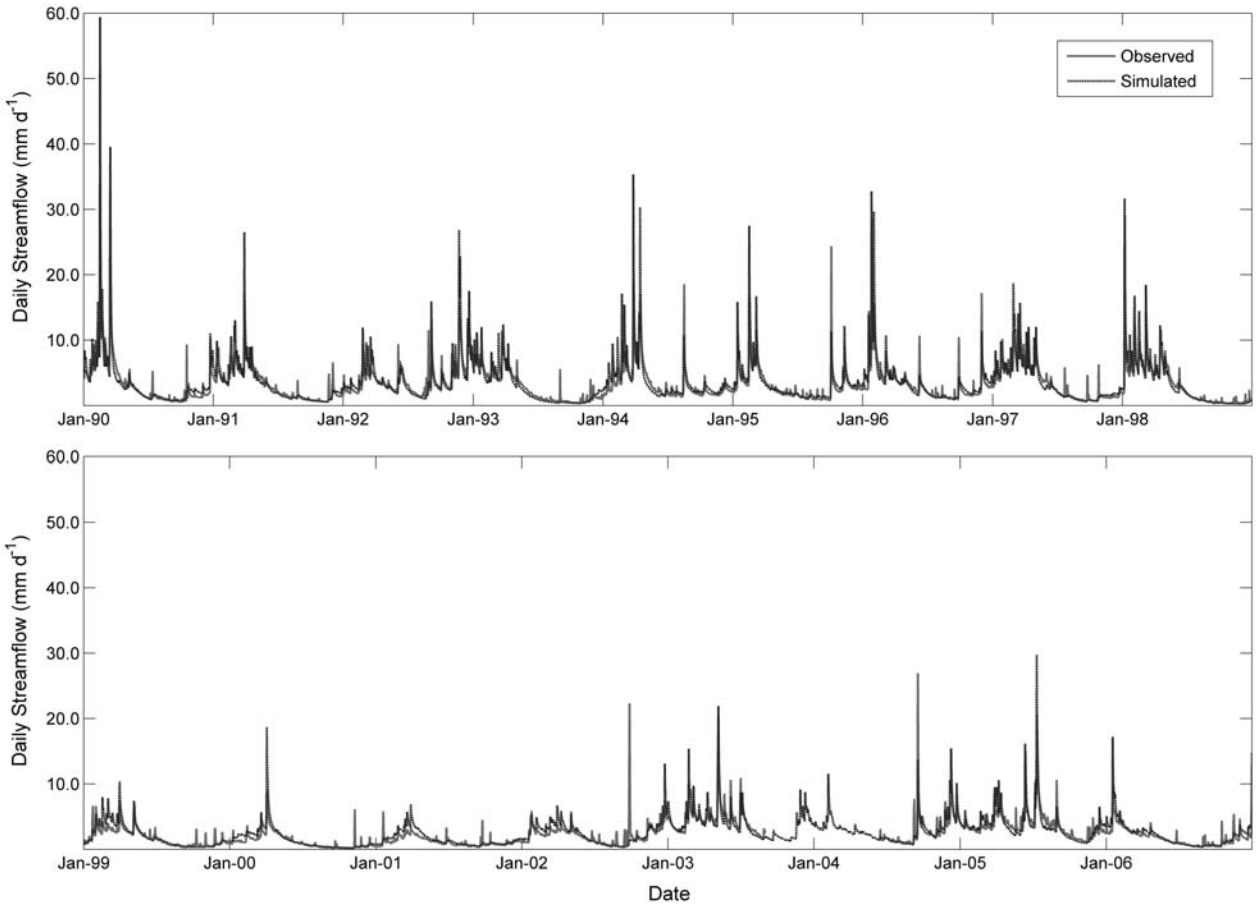

Figure 5. Long-term observed and simulated daily streamflow at the study watershed (1990 $\sim$ 2006), including the 3 year calibration period (October 1999 to September 2002).

[35] We show fairly good agreement between measured and simulated soil moisture content (1999 $\sim$ 2006) at upper 60 cm soil depth from three gradient plots that range from xeric to wet soil conditions (Figure 6). Therefore, reasonable spatiotemporal patterns of root zone moisture dynamics further constrains model parameterization in addition to streamflow data within the watershed.

[36] Figure 7 shows key long-term nitrogen transformation rates along the hillslope gradient, simulated based on the current vegetation gradients and the defined lateral hydrologic connectivity. In this area, nitrogen is cycled tightly with increasing mineralization and uptake rates downslope. A small proportion of available nitrogen is nitrified, with significant denitrification restricted to the wettest parts of the catchment. The difference in mineralization and plant N uptake is largely explained by atmospheric deposition (<1.0 g N m^{-2} y^{-1} [*Knoepp et al.*, 2008]), and fixation (1.1 g N m^{-2} y^{-1} [*Todd et al.*, 1975]). We point out that these gradients largely from in situ N cycling as we did not include lateral transport of mobile nitrogen (nitrate), or mass transport of organic litter downslope in the model version we used.

3.6. Prescribed Rooting Depth as a Function of Hillslope Position

[37] Lateral water flux through shallow soil columns is dominant in these mountainous forest catchments [*Hewlett and Hibbert*, 1963], which results in uneven distribution of plant available water along hydrologic flow paths [*Yeakley et al.*, 1998]. The spatial pattern of vegetation density within a watershed is a good estimator for spatial patterns of root zone moisture dynamics and lateral connectivity within watersheds. However, temporal dynamics of plant available water are dependent not only on hillslope position, but also on local properties like soil texture [*Porporato et al.*, 2001; *Brady and Weil*, 2002] and rooting depth [*Oren and Pataki*, 2001; *Schenk and Jackson*, 2002].

[38] We use maximum rooting depth in this study, rather than the usual definition of rooting depth (the depth of 95% cumulative distribution of root biomass [*Arora and Boer*, 2003]). Maximum rooting depth represents temporal dynamics of plant available water better as the deepest 5% of roots may play an important role for vegetation transpiration especially during a dry season [*Nepstad et al.*, 1994; *Canadell et al.*, 1996; *Jackson et al.*, 1999].

[39] Soil and vegetation may also vary systematically as a function of topographic position. Colluvial soil are thicker and slightly finer in wet and convergent topography with mesic species, but thinner and coarser in dry and divergent topography with xeric species in this area [*Day et al.*, 1988; *Yeakley et al.*, 1998; *Hales et al.*, 2009]. To reflect these local properties, a local rooting depth (*RD*) is expressed as a linear function of local wetness index (*WI*) with two rooting depth

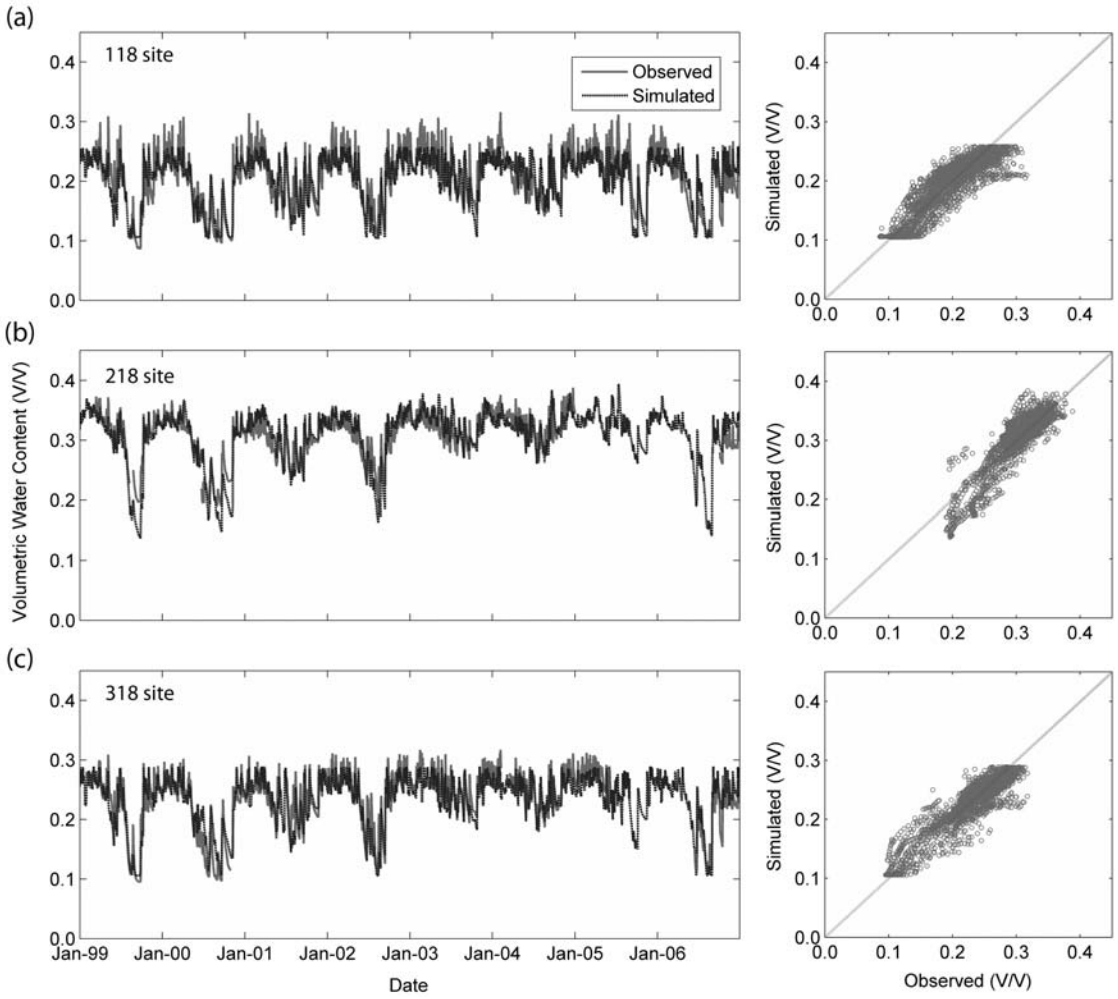

Figure 6. Time series and scatterplots of observed and simulated soil water content at (a) 118 (xeric), (b) 218 (mesic), and (c) 318 (intermediate) gradient plots within the target watershed.

parameters, average rooting depth (RD_{avg}) and spatial pattern of rooting depth (RD_{dev}):

$$RD = RD_{avg} + RD_{dev} \times \left(WI - WI_{avg}\right) \quad (10)$$

where WI_{avg} represents the average wetness index within the hillslope. The spatial pattern of rooting depth (RD_{dev}) parameter is the change in rooting depth with unit increase of wetness index, hence a positive value means increasing rooting depth in a downslope direction.

[40] Soil texture variation within the watershed is small, and we do not incorporate specific patterns in model parameterization. The model is then further calibrated by Monte Carlo sampling of RD_{avg} and RD_{dev} using degree of fit between simulated and estimated hydrologic gradients of vegetation density (Figure 4b). Different combinations of RD_{avg} and RD_{dev} result in variations in spatial patterns of LAI due to variations in water and nutrient availability, resulting photosynthesis, and allocation dynamics. The minimum rooting depth was set as 0.2 m to avoid numerical problems in the vertical hydrological processes in the model.

3.7. Allocation Dynamics With Varying Rooting Depth

[41] We used a constant allocation strategy between vegetation compartments (e.g., leaf, stem, fine root, coarse root) in the model, from the current BIOME-BGC algorithm [*Thornton*, 1998; *Thornton et al.*, 2002]. Allocation parameters are estimated from detailed field measurements of aboveground woody biomass increase, annual foliage productions, and root biomass dynamics around the study site (Table 3) [*McGinty*, 1976; *Day and Monk*, 1977; *Day et al.*, 1988]. Specifically, *McGinty* [1976] measured actual root growth dynamics by refilling three excavated pits over a two year period, providing information to calculate rough estimates for allocation ratios between vegetation compartments. He also measured the vertical distribution of root biomass in the mixed hardwood forest from twenty pits around the study area (WS14, WS22, WS27), from which we estimate maximum rooting depth.

[42] However, the allocation scheme can respond to local water availability, determined by a hillslope position and local properties. Many studies show that decreasing resource availability (water and nutrients) can favor partitioning more carbon belowground, in terms of climatic gradients [*Schenk and Jackson*, 2002; *Hui and Jackson*, 2006] and field experiments [*Cromer and Jarvis*, 1990; *Gedroc et al.*, 1996; *McConnaughay and Coleman*, 1999; *Ryan et al.*, 2004; *Litton et al.*, 2007]. For this reason, there is a long history of modeling efforts to integrate this dynamic allocation

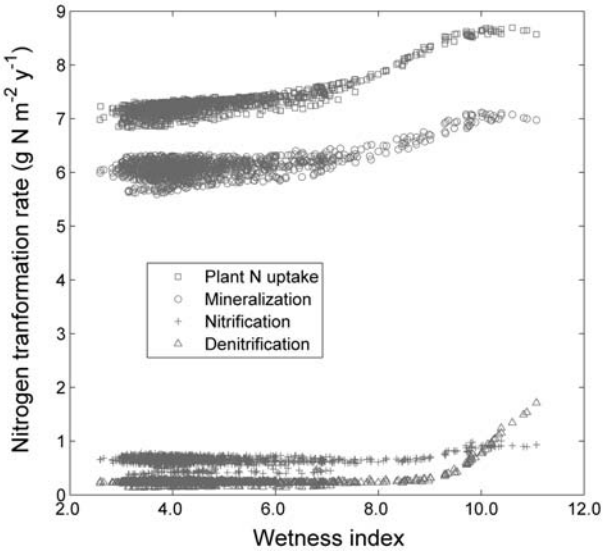

Figure 7. Simulated long-term (1941 ~ 2005) nitrogen transformation rates (plant uptake, mineralization, nitrification, and denitrification) in litter and soil as a function of wetness index. Note that these modeled gradients largely result from in situ N cycling as lateral transport of mobile nitrogen (nitrate), or organic litter downslope is not included in the simulation version. Each point represents a 10 × 10 m cell (n = 1253), a basic unit of model simulation.

scheme based on light, water, and nutrient availability [see *Wilson*, 1988; *Running and Gower*, 1991; *Friedlingstein et al.*, 1999; *Mackay*, 2001].

[43] In this study, we incorporated two kinds of allocation strategies. First, we used constant allocation parameters measured on site (Table 3) regardless of spatial patterns of prescribed rooting depth. Second, we simply assume the linear relationship between local rooting depth and constant belowground allocation ratios, which means that more fixed carbon is allocated to belowground with increasing prescribed local rooting depth. This alternative allocation strategy is justified by the fact that deeper roots require more belowground biomass. Under this alternative allocation strategy, if aboveground biomass remains the same, total belowground biomass is simply proportional to the rooting depth while it does not change under the constant allocation strategy. Following *Arora and Boer* [2003], this simple linear relationship between total belowground biomass and rooting depth assumes that roots grow mainly vertically downward while maintaining surface root density.

4. Results

4.1. Topographic Controls on Rooting Depth

[44] Figure 8 shows the difference of rooting depths and root distributions between ridge and hollow locations. Our data suggests that there is no significant difference in rooting depth between them, whether they are defined as 95% cumulative distribution of root counts (RD_{95}; Table 1) or maximum sampled roots depth (Figure 8). The average RD_{95} is 0.88 m in ridges (n = 8) and 0.91 m in hollows (n = 6). If we exclude coniferous (*Tsuga Canadensis*; hemlock) and evergreen (*Rhododendron maximum*; rhododendron) species and just compare deciduous forests, they are nearly equivalent (about 0.9 m). We note that maximum rooting depth is more error prone as roots are sampled in a two-dimensional face along a single pit which may miss individual deep roots such as tap roots.

[45] The average DBH for deciduous broadleaf species is 41.3 cm in hollows (n = 6) and 29.5 cm in ridges (n = 5) (Table 1), although this difference is dominated by a single large DBH stem (*Q. rubra*). *Bolstad et al.* [2001] also found general increases of aboveground biomass and leaf area from ridge to hollow from sixteen circular 0.1 ha plots with mixed deciduous hardwood stands in the Coweeta basin. *Martin et al.* [1998] found that DBH values from ten deciduous broadleaf species in the Coweeta basin have a linear allometric relationship with leaf area, estimated from leaf mass and specific leaf area (SLA) (R^2 = 0.822, n = 87). Therefore, although there is a 40% increase of LAI from ridge to hollow in this sample, maximum rooting depths remain almost constant.

4.2. Parameter Spaces

[46] Figure 9 indicates parameter spaces for RD_{avg} and RD_{dev} in regard to MAE (mean absolute error) values between simulated and estimated LAI from hydrologic gradients of vegetation (Figure 4b) for all patches (n = 1253). These parameter spaces are not much different if we use actual estimated LAI values from the IKONOS image directly, but much higher MAE values (>2.0) are expected even around the best fit parameter space.

[47] Best fit parameter spaces are very similar for both allocation strategies, where RD_{avg} is right above 0.8 m and RD_{dev} is around zero or very slightly positive values (Figure 9). Too shallow RD_{avg} or high RD_{dev} can result in steeper gradients of vegetation density along the hillslope than estimated ones, where local vegetation density is too dependent on hillslope positions. Instead, simulated spatial gradients of vegetation density can disappear at high RD_{avg} or low RD_{dev} ranges, where local vegetation density is a weaker function of hillslope positions. The patterns of MAE within parameter spaces are very different between two allocation strategies. As for constant allocation strategy, MAE increases very rapidly at shallow RD_{avg} ranges (Figure 9a), while it increases rapidly in the deeper RD_{avg} regions in alternative allocation strategy (Figure 9b).

[48] This range of estimated RD_{avg} is quite comparable to the actual maximum rooting depth measurements in the hardwood forest at the same northwest facing slopes around the study area [*McGinty*, 1976]. Roots measured at our pits are located in southeast facing slopes, so slightly higher maximum rooting depth values are reported. Nevertheless, we found very similar spatial pattern of rooting depth from pits excavation data (Table 1 and Figure 8), not so much different between topographic positions (ridges and hollows).

4.3. Long-Term Ecohydrologic Optimality at the Hillslope Scales

[49] Figures 10 and 11 show the simulated long-term mean annual NPP (net primary productivity) and ET (evapotranspiration) at the study watershed during the 65 year simulation period (1941 ~ 2005) with different rooting and allocation strategies. Annual ET is calculated on a water year basis to

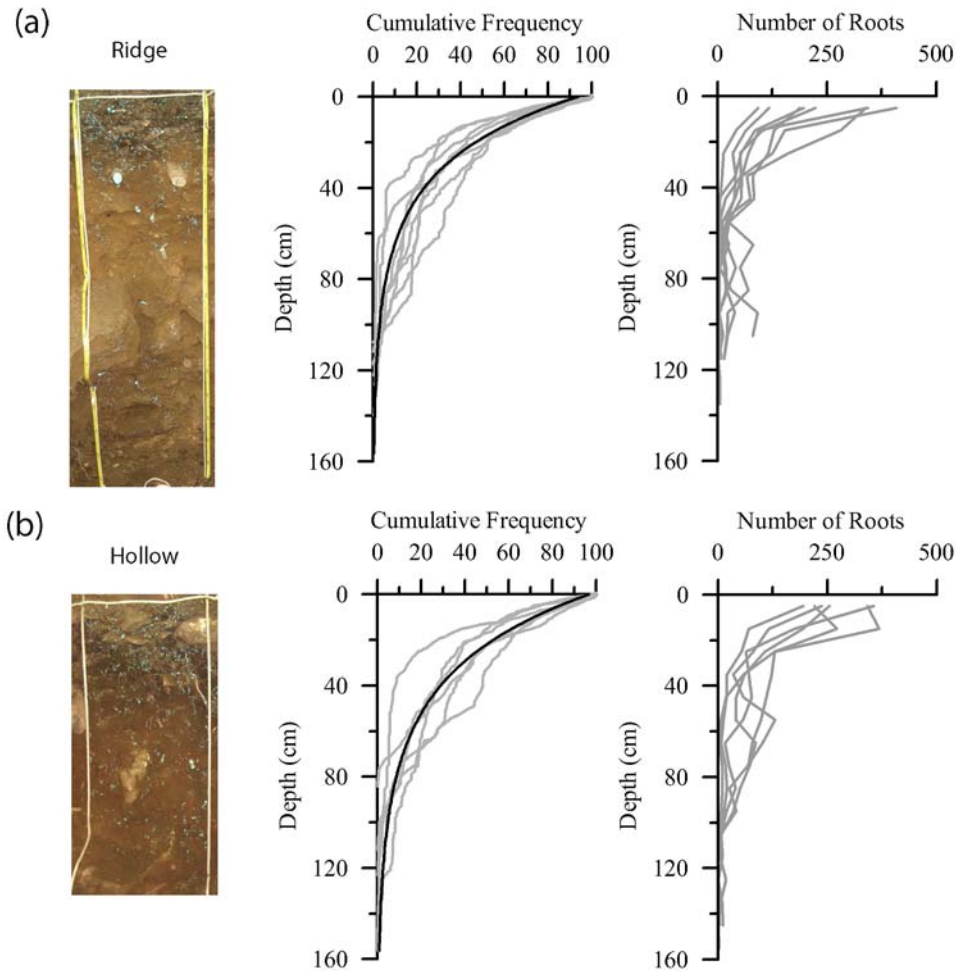

Figure 8. The distribution of roots as a function of soil depth for pits located on (a) ridges and (b) hollows. Distributions are expressed as root cumulative frequency and as absolute number. Grey lines represent individual pits, while black lines are the mean of all pits. Photographs are vertical sections of two *Q. rubra* pits (Table 1) dug within 20 m of each other. Note the difference in the depth of the dark A horizon between the two sites. Blue painted roots were used for analysis of root distributions. Modified from *Hales et al.* [2009, Figure 3].

compare with estimated ET from mass balance calculations (precipitation − runoff) at the catchment scale. Water use efficiency (WUE) values are calculated with total ET on an annual basis rather than transpiration to better represent the site level WUE [*Huxman et al.*, 2004]. Figure 12 shows how aboveground NPP (ANPP) changes with total NPP values under different allocation strategies, where ANPP to NPP ratios reflect model allocation ratios in the model. In the alternative allocation strategy, ANPP/NPP ratios start around one at a very shallow rooting depth and decline with increasing RD_{avg} (Figure 12b), but are invariant in the constant allocation strategy (Figure 12a). Simulated ANPP is useful not only to compare with the estimated ANPP values at the study site, but also to represent allocation to aboveground vegetation density (foliar biomass) in the long term simulations. LAI is not prescribed in the model, but a constant portion of cumulative ANPP is allocated into foliar biomass.

[50] For both allocation strategies, optimal carbon uptake occurs around the RD_{avg} with the best fit to the spatial gradients of vegetation density (based on measured and simulated LAI) within the watershed (Figure 9). Optimal carbon uptake ranges are simulated with RD_{dev} values slightly negative and very close to zero, similar to the RD_{dev} estimates. Maximum WUE values are also established around these parameter ranges for both allocation strategies.

[51] The simulated ANPP ranges at optimal parameter spaces (Figure 12) are similar to estimated long-term ANPP both at the whole catchment scale (419.5 g C m^{-2} y^{-1}) [*Day and Monk*, 1974, 1977; *Day et al.*, 1988] and at the plot scale [*Bolstad et al.*, 2001]. Also, note that there is significant discrepancy between optimal NPP and ANPP parameter ranges in the alternative allocation simulations (Figure 12b). Optimal ET ranges (Figures 10b and 11b) are a little lower than the catchment-scale estimated ET during the same period (794 mm y^{-1}). However, recent studies suggest that upscaled ET estimates from plot measurements in steep mountain catchments are lower than ET from mass balance, usually attributed to deep groundwater bypass [e.g., *Wilson et al.*, 2001]. *Ford et al.* [2007] also shows that 2 year ET estimates upscaled from detailed sap flux measurements are

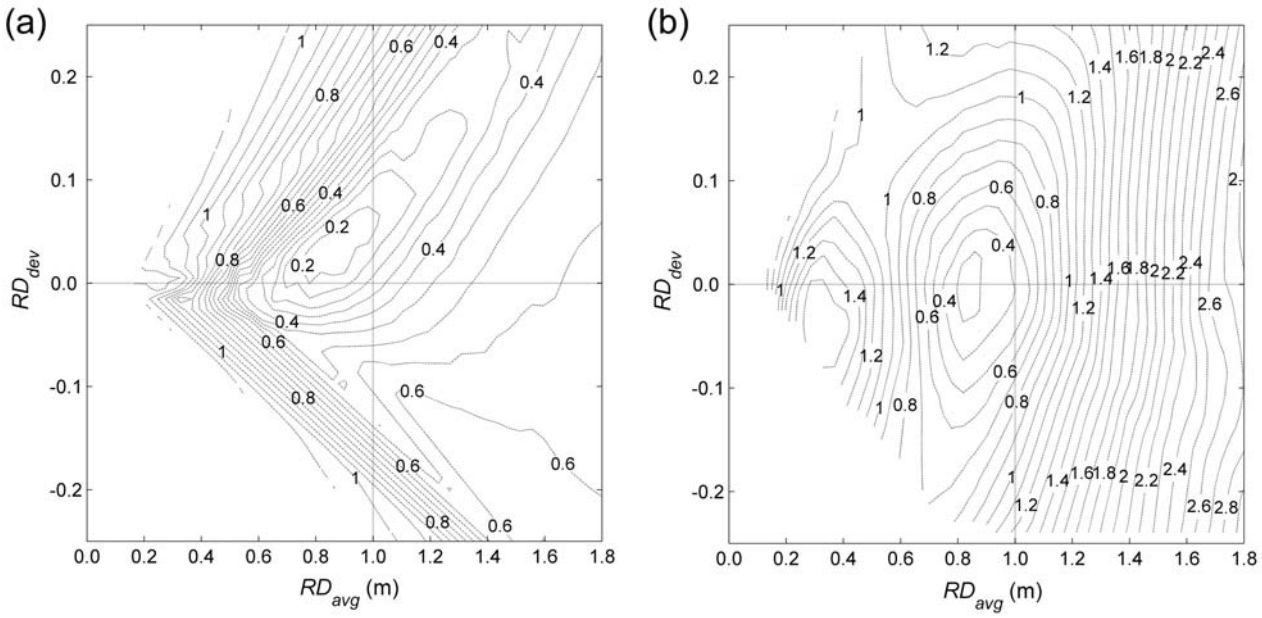

Figure 9. Mean absolute error (MAE) of simulated LAI within W18 over multiple realizations of average rooting depth (RD_{avg}) and spatial pattern of rooting depth (RD_{dev}) under (a) constant and (b) alternative allocation strategies.

about 10% lower than catchment-based estimated ET at the adjacent pair watershed (WS17; Figure 3c).

5. Discussion and Conclusions

5.1. Optimal Vegetation Gradients for System-Wide Productivity

[52] This study suggests that the existing hydrologic gradients of vegetation density measured within the watershed effectively represent the long-term optimal state for system-wide carbon uptake. Model parameters controlling lateral hydrologic connectivity of the watershed are first calibrated from long-term streamflow data, which also produces reasonable spatiotemporal dynamics of surface soil moisture. To investigate the optimality of vegetation gradients, multiple spatial patterns of vegetation within the watershed are simulated by varying rooting depth as a function of hillslope position. Optimal ranges of rooting depth parameters are also supported by field measurements from pits excavation. Two different allocation strategies in the simulations elaborate the importance of canopy carbon allocation to the emergent optimality as a function of vegetation canopy patterns.

[53] Less vegetation upslope produces a subsidy of more water to downslope vegetation, where more water and nitrogen are available. Model results suggest that more efficient photosynthesis can take place downslope for two reasons. First, increased nitrogen availability can increase carbon uptake per unit water loss (water use efficiency) in downslope vegetation. Second, ample soil moisture downslope allows plants to allocate proportionately less carbon into belowground biomass and more into aboveground, which increases leaf area, light absorption, and total carbon uptake. However, steeper vegetation gradients (sparser canopy upslope, denser downslope) than the existing canopy pattern simulated by decreasing RD_{avg} or increasing RD_{dev} (Figure 9), provide a water subsidy from upslope that exceeds the capacity of the downslope canopy to transpire following an asymptotic response of ET to available water. This results in less total ET and greater catchment runoff ratios (Figures 10b and 11b).

[54] Uniform or inverse vegetation gradients are established by increasing RD_{avg} or decreasing RD_{dev} (Figure 9), with system-wide declines of carbon uptake for two different allocation strategies. With the constant allocation strategy, greater upslope water uptake provides less water subsidy downslope, resulting in increased total catchment ET. However, catchment productivity does not follow increasing plant water uptake because of lower nitrogen availability, specifically in upslope regions (Figure 7). Less nitrogen availability can result from decreases both in nitrogen transformation rates and limited amount of nitrogen upslope in the model. Second, with the alternative allocation strategy (greater proportional belowground allocation of photosynthate with increasing rooting depth), total ET and NPP decline with limited light availability (lower canopy light absorption).

[55] In summary, the current vegetation density gradients can result from self-organization for optimal carbon uptake between adjacent patches along flow paths. They may effectively represent the degree of dependency of multiple interacting resources (water and nutrients), moderated by feedbacks with canopy light absorption. Therefore, vegetation pattern along hydrologic flow paths is a function of lateral hydrologic connectivity within the hillslope.

5.2. Compromises Between Multiple Resources

[56] Competition for light, water, and nutrients are the most important factors determining allocation of fixed carbon into vegetation compartments, providing the ecophysiologic basis for compromising between multiple stresses for optimal carbon uptake [*Tilman*, 1988; *Gedroc et al.*, 1996; *McConnaughay and Coleman*, 1999]. Simulated optimal carbon uptake ranges in this study show effective compro-

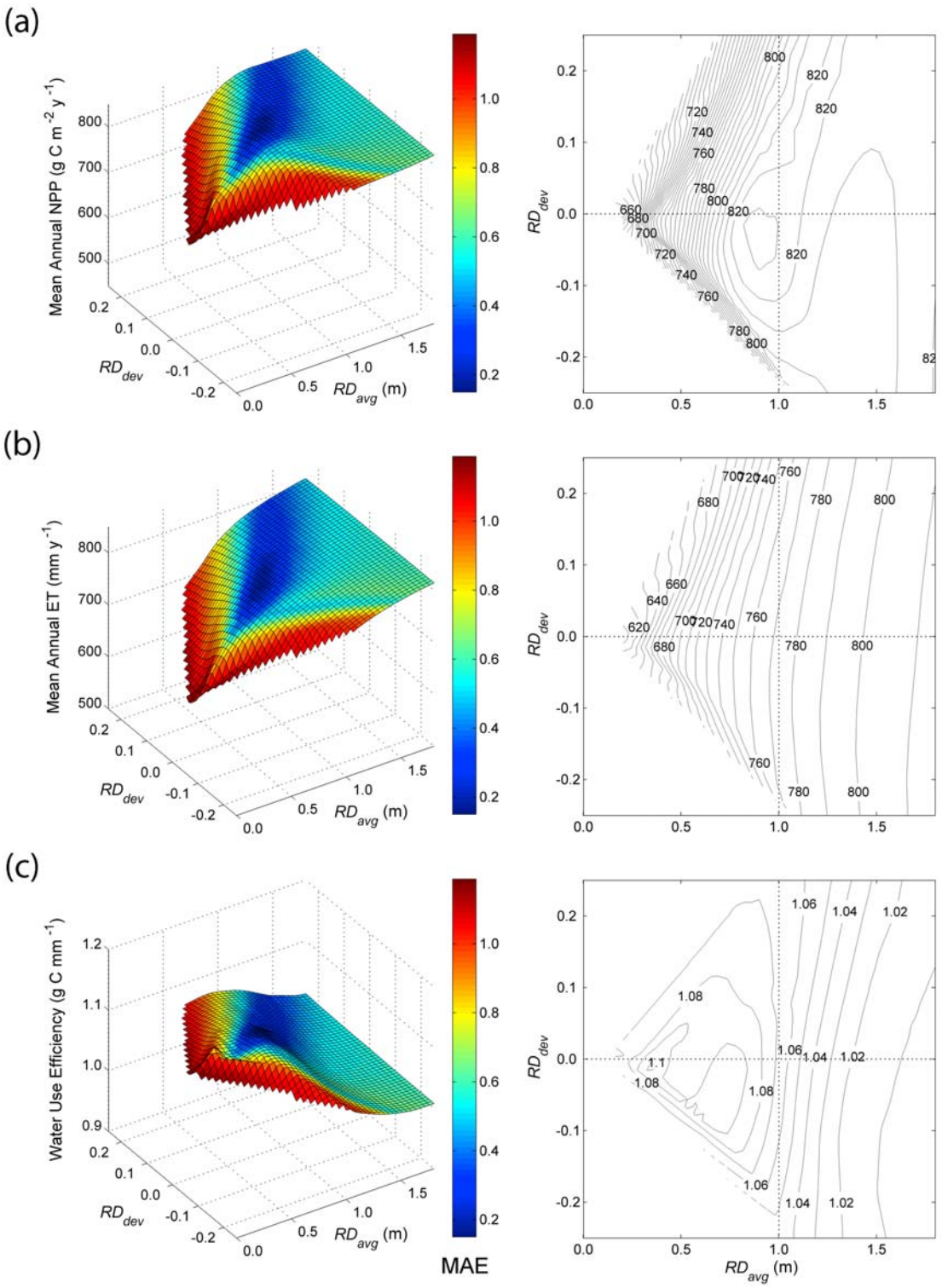

Figure 10. Three- and two-dimensional contour plots of long-term simulated (1941 ∼ 2005) average annual (a) net primary productivity (NPP), (b) evapotranspiration (ET), and (c) water used efficiency (WUE) over sampled RD_{avg} and RD_{dev} under constant allocation strategy. The color bar represents MAE of simulated LAI (Figure 9a).

mises between multiple stresses (water, light, and nutrients) for optimal carbon uptake. For both of the allocation strategies, there are water-limited productivity conditions up to optimal RD_{avg} ranges, whereas different stress terms act as a limiting factor for carbon uptake above optimal RD_{avg} ranges.

[57] With the constant allocation strategy, catchment scale NPP is fairly steady above optimal RD_{avg} ranges even though

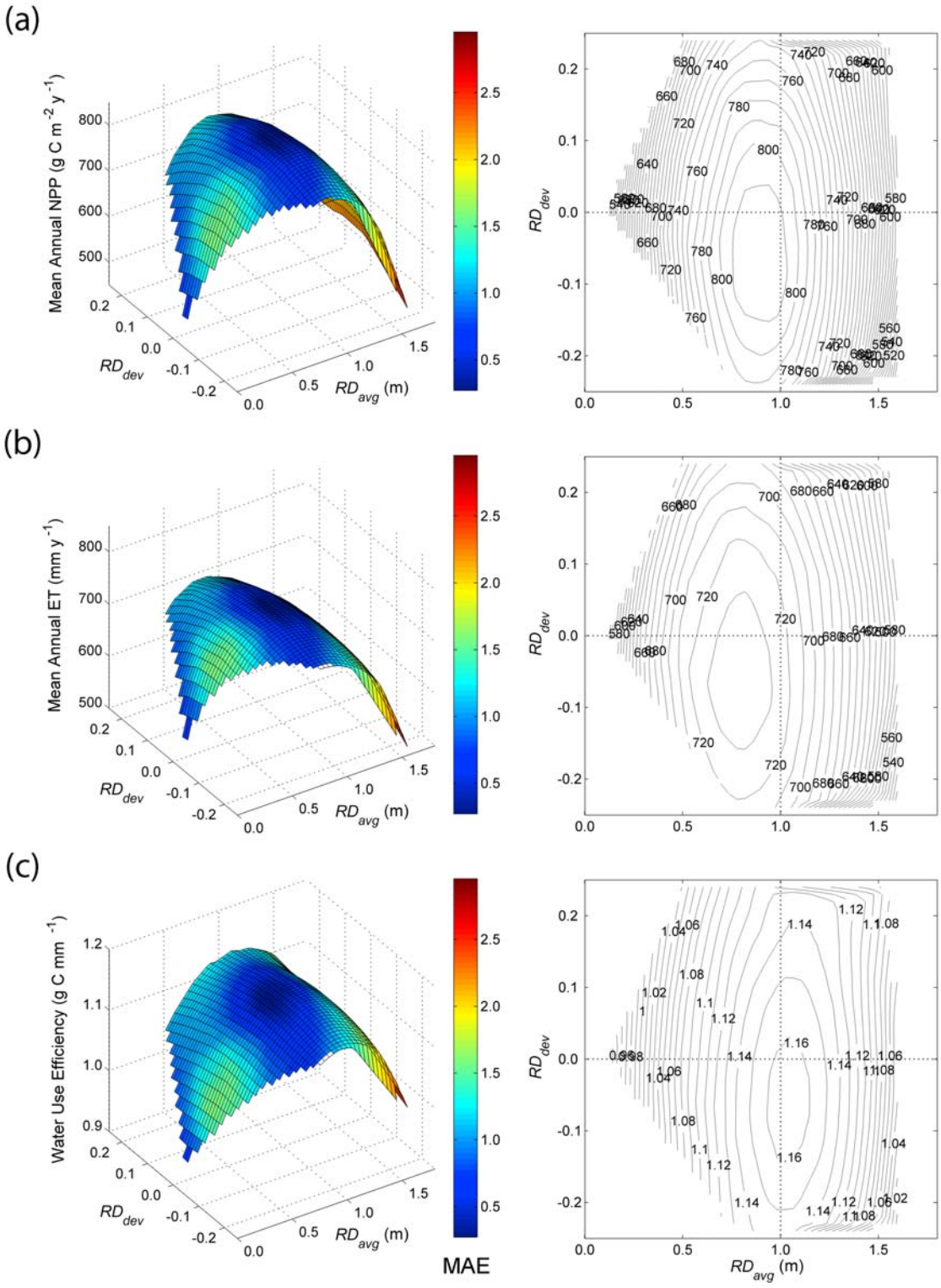

Figure 11. 3 Three- and two-dimensional contour plots of long-term simulated (1941 $\sim$ 2005) average (a) net primary productivity (NPP), (b) evapotranspiration (ET), and (c) water used efficiency (WUE) over sampled RD_{avg} and RD_{dev} under alternative allocation strategy, where allocation ratios are as a function of local rooting depth. The color bar represents MAE of simulated LAI (Figure 9b).

annual mean ET increases (Figure 10). This increase of ET is mainly attributed to transpiration with increasing local rooting depth, not evaporation (interception), as LAI (following ANPP) remains almost constant (Figure 12a). This is mainly explained by decreasing nitrogen availability with increasing RD_{avg} especially in upslope regions (Figure 7). More localized soil water uptake with increasing local rooting depths requires more nitrogen especially upslope, which however is

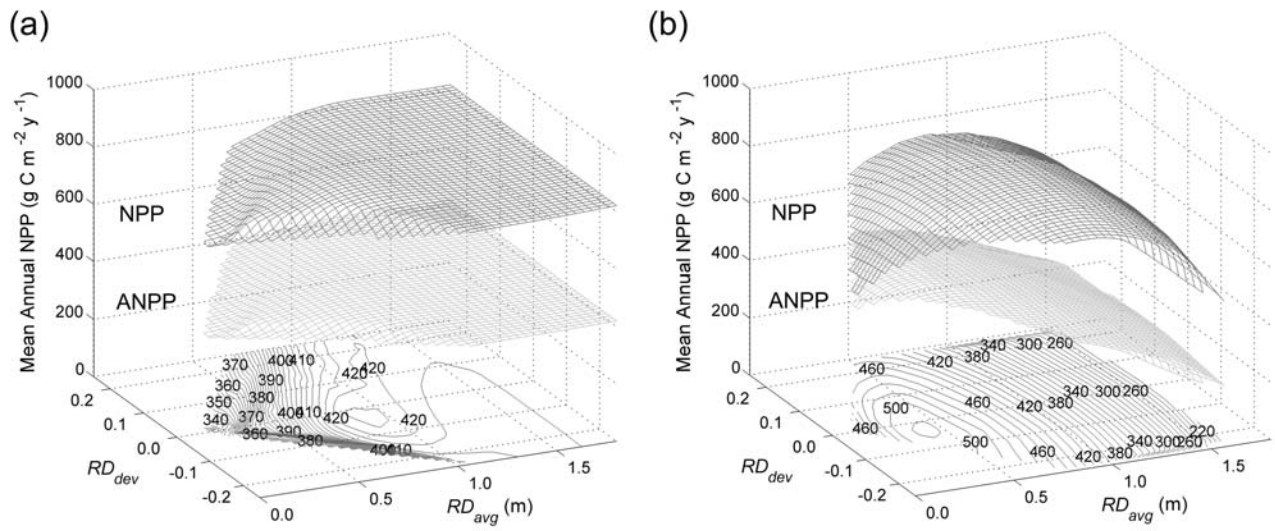

Figure 12. Three-dimensional plots for long-term annual net primary productivity (NPP) and aboveground NPP (ANPP) under (a) constant and (b) alternative allocation strategies with varying RD_{avg} and RD_{dev} parameters. Contours at the *x*-*y* plane represent ANPP values. Note that allocation ratios of ANPP to NPP are constant under constant allocation strategy, while they decrease in proportion to rooting depth under alternative allocation strategy. Long-term patterns of vegetation density (LAI) follow ANPP as a constant portion of cumulative ANPP is allocated into foliar biomass.

not available. In the model, nitrogen is assumed to be confined within specified rooting depth. Therefore, increased root depth produces more water availability but not nitrogen. Rather, wetter root zone moisture dynamics reduce N transformation rates as upper 60 cm soil moisture ranges within the study site are already very close to the levels maximizing decomposition, mineralization, and nitrification rates in soils highest (around 60% saturation for sandy loam soils, Figures 1 and 6), except for short dry seasons. The decline of nitrogen availability results in consistent decreases of WUE above optimal RD_{avg} ranges (Figure 10c). In contrast, for the alternative allocation strategy carbon uptake and annual ET decline quickly above the optimal RD_{avg} ranges (Figure 11). Deeper rooting depth increases water availability, while increased proportional belowground carbon allocation limits foliar biomass which decreases light absorption (Figure 12b).

[58] Significant discrepancy between optimal NPP and ANPP parameter ranges in the alternative allocation simulations (Figure 12b) shows an example of effective compromise between light and water resources for optimal system-wide carbon uptake (NPP). Allocation of limited photosynthate into vegetation compartments (e.g., foliar, root), is related to trade-off between resources (e.g., light, water), for a plant would be increasing one resource availability by decreasing the other [*Tilman*, 1988]. For example, even though there is higher aboveground vegetation density (or higher light availability) by more aboveground allocation at shallower RD_{avg} ranges (around 0.4 m), catchment scale optimal carbon uptake is limited by water stress, driven by lower belowground allocation. This suggests that the "growth-stress trade-off" concept should be regarded as a compromise between two main complementary resources (light and water) for optimal carbon uptake itself through the control of aboveground vegetation density by limited photosynthate allocation [*Tilman*, 1988; *Gedroc et al.*, 1996; *McConnaughay and Coleman*, 1999].

5.3. Allocation Dynamics Along the Hillslope Gradients

[59] It is widely accepted that proportional belowground allocation usually increases with decreasing water and nutrient availability [*Cromer and Jarvis*, 1990; *Gedroc et al.*, 1996; *Friedlingstein et al.*, 1999; *McConnaughay and Coleman*, 1999; *Ryan et al.*, 2004; *Litton et al.*, 2007]. In WS18, surface soil moisture dynamics (Figure 6) indicate that wetter regions are more favorable to available nitrogen along with associated nutrient transport through shallow subsurface flow. Moreover, soil moisture has a primary control on vegetation density (Figure 4b), which suggests that the amount of nitrogen input through litter inputs also follows hillslope gradients. For these reasons, there are significant increases of nitrogen availability with wetness within the study site [*Knoepp and Swank*, 1998; *Knoepp et al.*, 2008], which also suggests a more rapid cycling of organic matter and greater amount of nutrients available to plants. Therefore, the belowground allocation proportion may decrease with hillslope moisture gradients (without a species shift) simply because water and nutrient availability increases.

[60] This spatial allocation pattern is very similar to what we found in pits excavation experiments (Figure 8) and the alternative allocation strategy simulations (Figure 11) with spatially homogeneous vegetation species. There was significant increase of DBH from ridge to hollow in our sample, maximum rooting depths are almost constant (Table 1). Even though we did not actually calculate total belowground biomass for the lack of lateral roots spread information, this shows possible transitions in allocation dynamics along the hillslope gradients. In the simulation, the optimal RD_{dev}

parameter for optimal carbon uptake is located at slightly negative ranges, so maximum rooting depth and belowground allocation proportion slightly decreases downslope. However, transitions into more tolerant vegetation species in a dry region may offset this optimal allocation dynamics along the hillslope gradient. As far as we know, there are no empirical studies on the allocation dynamics along hillslope gradients, that account for the effects of downslope changes of water, nutrients, light availability [*McConnaughay and Coleman*, 1999, and references therein], species shifts [*McConnaughay and Coleman*, 1999; *Gower et al.*, 2001], and stand ages (often called "ontogenic drift") [*Coleman and McConnaughay*, 1995; *Ryan et al.*, 2004; *Litton et al.*, 2007]. For this reason, it would be difficult to find consistent allocation patterns along hillslope gradients in natural situations.

5.4. Limitations of This Study

[61] In this study, we used a simple representation of rooting depth given the complexity of spatial variation and transport processes, assuming density to be evenly distributed with depth. However, a vertical distribution of roots is important for determining water and nutrient availability [*Jackson et al.*, 2000; *Collins and Bras*, 2007]. Shallow roots play an important role in nutrient recycling as most nutrients (especially nitrogen) are concentrated in the surface soil layer [*Jobbagy and Jackson*, 2001], while deep roots mostly determine water availability during a dry season. For this reason, vertical distribution of roots can play an important role in compromising between these two resources (water and nutrients). Pit observations in our site show fine roots are more evenly distributed with depth in hollow soils, while fine roots often show bimodal distributions at shallow soil depth and the soil-saprolite boundary [*Hales et al.*, 2009]. A feedback between greater carbon allocation to deeper roots and the density of shallow fine roots may be useful to explore in future modeling efforts. However, this would require significantly more information on soil profile form and computational effort, especially if multiple model realizations are required.

[62] Second, we did not integrate detailed spatial patterns of vegetation species and soil in the study area. Vegetation species varies from xeric to mesic species following hillslope position in this study site [*Day and Monk*, 1974; *Day et al.*, 1988]. Xeric species are more tolerant to water stress, so optimal carbon uptake may occur at shallower rooting depth than simulated by the model in upslope regions. Mesic species need more water, so optimal carbon uptake may occur at deeper rooting depth than simulated in downslope regions. Hence optimal rooting depth patterns (RD_{dev}) may show a small positive trend downslope given the spatial pattern of species transition. We note that in both simulated and observed rooting depth, trends are close to zero, contrary to our initial expectations. However, this trend is consistent with the trend of the absolute amount of photosynthate production and the proportional aboveground/belowground allocation.

[63] In the study catchment, soil texture varies from fine sandy loam to silt loam (from soil texture data provided by Todd Lookingbill) with increasing wetness along the hillslope gradients, while soil tends from thinner to thicker [*Hales et al.*, 2009]. However, out soil pit observations did not indicate any strong textural gradients, but did reveal large local heterogeneity in colluvial soils. Transition of soil texture along the hillslope gradients may favor soil water holding capacity in wetter regions per unit soil depth [*Brady and Weil*, 2002; *Dingman*, 2002; *Schenk and Jackson*, 2005]. However, *Hales et al.* [2009] also found high fine root density profiles in the soil-saprolite boundaries in dry region. This suggests that soil-saprolite boundary acts as a physical barrier for deep roots in the dry region, in which case optimal rooting depth patterns may not be properly established along the hillslope gradients.

5.5. Conclusions

[64] This study suggests that the existing hydrologic gradients of vegetation within the catchment effectively represent the long-term optimal state for carbon uptake, which is closely modulated by rooting and allocation strategies. Traditionally, optimality approaches have assumed a steady state mechanism within the model, based on water or carbon principles. We have used a different approach emphasizing a fully transient, distributed model to investigate whether optimal ecosystem properties emerge as a result of self organizing spatial patterns of canopy density, specifically in the form of catchment scale ecosystem productivity and water use efficiency. The existing vegetation pattern must be understood as a feedback between multiple stresses (e.g., light, water, and nutrients) as connected by water flow along topographic gradients. This adjustment and evolution of the ecosystem with the geomorphic, climatic and hydrologic settings results in an emergent pattern that optimizes system-wide carbon uptake, over and above the individual patch. This study extends and tests the concept of ecophysiological optimality theory at short-term and plot scales to long-term ecohydrological optimality at catchment and hillslope scales.

[65] **Acknowledgments.** The research represented in this paper was supported by a USDA Forest Service cooperative agreement (SRS-06-CA 11330410-0) and the National Science Foundation award to the Coweeta Long-term Ecologic Research project (DEB 0823293). Data were made available from the Coweeta Hydrological Laboratory and LTER, which is supported by the National Science Foundation and the USDA Forest Service. We specifically thank Jim Vose and Paul Bolstad for their support in providing data in the Coweeta Hydrologic Lab. We also thank Todd Lookingbill, who provided the valuable soil information.

References

Arora, V. K., and G. J. Boer (2003), A representation of variable root distribution in dynamic vegetation models, *Earth Interact.*, *7*, 1–19, doi:10.1175/1087-3562(2003)007<0001:AROVRD>2.0.CO;2.

Arris, L. L., and P. S. Eagleson (1994), A water-use model for locating the boreal deciduous forest ecotone in eastern North America, *Water Resour. Res.*, *30*, 1–9, doi:10.1029/93WR02746.

Baldocchi, D. D., R. J. Luxmoore, and J. L. Hatfield (1991), Discerning the forest from the trees—An essay on scaling canopy stomatal conductance, *Agric. For. Meteorol.*, *54*, 197–226, doi:10.1016/0168-1923(91)90006-C.

Band, L. E., P. Patterson, R. Nemani, and S. W. Running (1993), Forest ecosystem processes at the watershed scale: Incorporating hillslope hydrology, *Agric. For. Meteorol.*, *63*, 93–126, doi:10.1016/0168-1923(93)90024-C.

Band, L. E., C. L. Tague, P. Groffman, and K. Belt (2001), Forest ecosystem processes at the watershed scale: Hydrological and ecological controls of nitrogen export, *Hydrol. Processes*, *15*, 2013–2028, doi:10.1002/hyp.253.

Beven, K., and M. Kirkby (1979), A physically based variable contributing area model of basin hydrology, *Hydrol. Sci. Bull.*, *24*, 43–69.

Bolstad, P. V., and J. M. Vose (2005), Forest and pasture carbon pools and soil respiration in the southern Appalachian Mountains, *For. Sci.*, *51*, 372–383.

Bolstad, P. V., K. Mitchell, and J. M. Vose (1999), Foliar temperature-respiration response functions for broad-leaved tree species in the southern Appalachians, *Tree Physiol.*, *19*, 871–878.

Bolstad, P. V., J. M. Vose, and S. G. McNulty (2001), Forest productivity, leaf area, and terrain in southern Appalachian deciduous forests, *For. Sci.*, *47*, 419–427.

Brady, N. C., and R. R. Weil (2002), *The Nature and Properties of Soils*, 13th ed., Prentice Hall, Upper Saddle River, N. J.

Bromley, J., J. Brouwer, A. P. Barker, S. R. Gaze, and C. Valentin (1997), The role of surface water redistribution in an area of patterned vegetation in a semi-arid environment, south-west Niger, *J. Hydrol.*, *198*, 1–29, doi:10.1016/S0022-1694(96)03322-7.

Camporeale, C., and L. Ridolfi (2006), Riparian vegetation distribution induced by river flow variability: A stochastic approach, *Water Resour. Res.*, *42*, W10415, doi:10.1029/2006WR004933.

Canadell, J., R. B. Jackson, J. R. Ehleringer, H. A. Mooney, O. E. Sala, and E. D. Schulze (1996), Maximum rooting depth of vegetation types at the global scale, *Oecologia*, *108*, 583–595, doi:10.1007/BF00329030.

Caylor, K. K., T. M. Scanlon, and I. Rodriguez-Iturbe (2004), Feasible optimality of vegetation patterns in river basins, *Geophys. Res. Lett.*, *31*, L13502, doi:10.1029/2004GL020260.

Caylor, K. K., S. Manfreda, and I. Rodriguez-Iturbe (2005), On the coupled geomorphological and ecohydrological organization of river basins, *Adv. Water Resour.*, *28*, 69–86, doi:10.1016/j.advwatres.2004.08.013.

Chen, J. M., and J. Cihlar (1996), Retrieving leaf area index of boreal conifer forests using Landsat TM images, *Remote Sens. Environ.*, *55*, 153–162, doi:10.1016/0034-4257(95)00195-6.

Chen, J. M., J. Liu, J. Cihlar, and M. L. Goulden (1999), Daily canopy photosynthesis model through temporal and spatial scaling for remote sensing applications, *Ecol. Modell.*, *124*, 99–119, doi:10.1016/S0304-3800(99)00156-8.

Chen, J. M., X. Y. Chen, W. M. Ju, and X. Y. Geng (2005), Distributed hydrological model for mapping evapotranspiration using remote sensing inputs, *J. Hydrol.*, *305*, 15–39, doi:10.1016/j.jhydrol.2004.08.029.

Clinton, B. D., J. A. Yeakley, and D. K. Apsley (2003), Tree growth and mortality in a southern Appalachian deciduous forest following extended wet and dry periods, *Castanea*, *68*, 189–200.

Coleman, J. S., and K. D. M. McConnaughay (1995), A non-functional interpretation of a classical optimal-partitioning example, *Funct. Ecol.*, *9*, 951–954.

Collatz, G. J., J. T. Ball, C. Grivet, and J. A. Berry (1991), Physiological and environmental-regulation of stomatal conductance, photosynthesis and transpiration—A model that includes a laminar boundary layer, *Agric. For. Meteorol.*, *54*, 107–136, doi:10.1016/0168-1923(91)90002-8.

Collins, D. B. G., and R. L. Bras (2007), Plant rooting strategies in water-limited ecosystems, *Water Resour. Res.*, *43*, W06407, doi:10.1029/2006WR005541.

Cowan, I. R. (1982), Regulation of water use in relation to carbon gain in higher plants, in *Physical Plant Ecology II*, vol. 12, edited by O. L. Lange et al., pp. 589–613, Springer, Berlin.

Cowan, I. R., and G. D. Farquhar (1977), Stomatal function in relation to leaf metabolism and environment, in *Integration of Activity in the Higher Plant*, edited by D. H. Jennings, pp. 471–505, Cambridge Univ. Press, Cambridge, U. K.

Creed, I. F., and L. E. Band (1998a), Exploring functional similarity in the export of nitrate-N from forested catchments: A mechanistic modeling approach, *Water Resour. Res.*, *34*, 3079–3093, doi:10.1029/98WR02102.

Creed, I. F., and L. E. Band (1998b), Export of nitrogen from catchments within a temperate forest: Evidence for a unifying mechanism regulated by variable source area dynamics, *Water Resour. Res.*, *34*, 3105–3120, doi:10.1029/98WR01924.

Cromer, R. N., and P. G. Jarvis (1990), Growth and biomass partitioning in Eucalyptus-grandis seedlings in response to nitrogen supply, *Aust. J. Plant Physiol.*, *17*, 503–515.

Day, F. P., and C. D. Monk (1974), Vegetation patterns on a southern Appalachian watershed, *Ecology*, *55*, 1064–1074, doi:10.2307/1940356.

Day, F. P., and C. D. Monk (1977), Net primary production and phenology on a southern Appalachian watershed, *Am. J. Bot.*, *64*, 1117–1125, doi:10.2307/2442168.

Day, F. P., D. L. Philips, and C. D. Monk (1988), Forest communities and patterns, in *Forest Hydrology and Ecology at Coweeta*, edited by W. T. Swank and D. A. Crossley Jr., pp. 141–149, Springer, New York.

de Pury, D. G. G., and G. D. Farquhar (1997), Simple scaling of photosynthesis from leaves to canopies without the errors of big-leaf models, *Plant Cell Environ.*, *20*, 537–557, doi:10.1111/j.1365-3040.1997.00094.x.

Dingman, S. L. (2002), *Physical Hydrology*, 2nd ed., Prentice Hall, Upper Saddle River, N. J.

Eagleson, P. S. (1978a), Climate, soil, and vegetation: 1. Introduction to water balance dynamics, *Water Resour. Res.*, *14*, 705–712, doi:10.1029/WR014i005p00705.

Eagleson, P. S. (1978b), Climate, soil, and vegetation: 2. Distribution of annual precipitation derived from observed storm sequences, *Water Resour. Res.*, *14*, 713–721, doi:10.1029/WR014i005p00713.

Eagleson, P. S. (1978c), Climate, soil, and vegetation: 3. Simplified model of soil moisture movement in liquid phase, *Water Resour. Res.*, *14*, 722–730, doi:10.1029/WR014i005p00722.

Eagleson, P. S. (1978d), Climate, soil, and vegetation: 4. Expected value of annual evapotranspiration, *Water Resour. Res.*, *14*, 731–739, doi:10.1029/WR014i005p00731.

Eagleson, P. S. (1978e), Climate, soil, and vegetation: 5. Derived distribution of storm surface runoff, *Water Resour. Res.*, *14*, 741–748, doi:10.1029/WR014i005p00741.

Eagleson, P. S. (1978f), Climate, soil, and vegetation: 6. Dynamics of annual water balance, *Water Resour. Res.*, *14*, 749–764, doi:10.1029/WR014i005p00749.

Eagleson, P. S. (1978g), Climate, soil, and vegetation: 7. Derived distribution of annual water yield, *Water Resour. Res.*, *14*, 765–776, doi:10.1029/WR014i005p00765.

Eagleson, P. S. (1982), Ecological optimality in water-limited natural soil-vegetation systems: 1. Theory and hypothesis, *Water Resour. Res.*, *18*, 325–340, doi:10.1029/WR018i002p00325.

Eagleson, P. S. (2002), *Ecohydrology*, Cambridge Univ. Press, New York.

Eagleson, P. S., and T. E. Tellers (1982), Ecological optimality in water-limited natural soil-vegetation systems: 2. Tests and applications, *Water Resour. Res.*, *18*, 341–354, doi:10.1029/WR018i002p00341.

Elliott, K. J., and W. T. Swank (1994), Impacts of drought on tree mortality and growth in a mixed hardwood forest, *J. Veg. Sci.*, *5*, 229–236, doi:10.2307/3236155.

Emanuel, R. E., P. D'Odorico, and H. E. Epstein (2007), Evidence of optimal water use by vegetation across a range of North American ecosystems, *Geophys. Res. Lett.*, *34*, L07401, doi:10.1029/2006GL028909.

Famiglietti, J. S., and E. F. Wood (1994), Application of multiscale water and energy-balance models on a tallgrass prairie, *Water Resour. Res.*, *30*, 3079–3093, doi:10.1029/94WR01499.

Farquhar, G. D., and S. von Caemmerer (1982), Modeling of photosynthetic response to environmental conditions, in *Physical Plant Ecology II*, vol. 12, edited by O. L. Lange et al., pp. 550–587, Springer, Berlin.

Farquhar, G. D., S. V. Caemmerer, and J. A. Berry (1980), A biochemical model of photosynthetic CO_2 assimilation in leaves of C_3 species, *Planta*, *149*, 78–90, doi:10.1007/BF00386231.

Farquhar, G. D., S. von Caemmerer, and J. A. Berry (2001), Models of photosynthesis, *Plant Physiol.*, *125*, 42–45, doi:10.1104/pp.125.1.42.

Fassnacht, K. S., S. T. Gower, M. D. MacKenzie, E. V. Nordheim, and T. M. Lillesand (1997), Estimating the leaf area index of north central Wisconsin forests using the Landsat Thematic Mapper, *Remote Sens. Environ.*, *61*, 229–245, doi:10.1016/S0034-4257(97)00005-9.

Field, C. (1983), Allocating leaf nitrogen for the maximization of carbon gain: Leaf age as a control on the allocation program, *Oecologia*, *56*, 341–347, doi:10.1007/BF00379710.

Ford, C. R., R. M. Hubbard, B. D. Kloeppel, and J. M. Vose (2007), A comparison of sap flux-based evapotranspiration estimates with catchment-scale water balance, *Agric. For. Meteorol.*, *145*, 176–185, doi:10.1016/j.agrformet.2007.04.010.

Friedlingstein, P., G. Joel, C. B. Field, and I. Y. Fung (1999), Toward an allocation scheme for global terrestrial carbon models, *Global Change Biol.*, *5*, 755–770, doi:10.1046/j.1365-2486.1999.00269.x.

Friend, A. D., A. K. Stevens, R. G. Knox, and M. G. R. Cannell (1997), A process-based, terrestrial biosphere model of ecosystem dynamics (Hybrid v3.0), *Ecol. Modell.*, *95*, 249–287, doi:10.1016/S0304-3800(96)00034-8.

Gedroc, J. J., K. D. M. McConnaughay, and J. S. Coleman (1996), Plasticity in root shoot partitioning: Optimal, ontogenetic, or both?, *Funct. Ecol.*, *10*, 44–50, doi:10.2307/2390260.

Gholz, H. L., S. A. Vogel, W. P. Cropper, K. McKelvey, K. C. Ewel, R. O. Teskey, and P. J. Curran (1991), Dynamics of canopy structure and light interception in *Pinus elliottii* stands, north Florida, *Ecol. Monogr.*, *61*, 33–51, doi:10.2307/1942998.

Gower, S. T., and J. M. Norman (1991), Rapid estimation of leaf area index in conifer and broad-leaf plantations, *Ecology*, *72*, 1896–1900, doi:10.2307/1940988.

Gower, S. T., O. Krankina, R. J. Olson, M. Apps, S. Linder, and C. Wang (2001), Net primary production and carbon allocation patterns of boreal forest ecosystems, *Ecol. Appl.*, *11*, 1395–1411, doi:10.1890/1051-0761(2001)011[1395:NPPACA]2.0.CO;2.

Guswa, A. J. (2008), The influence of climate on root depth: A carbon cost-benefit analysis, *Water Resour. Res.*, *44*, W02427, doi:10.1029/2007WR006384.

Hales, T. C., C. R. Ford, T. Hwang, J. M. Vose, and L. E. Band (2009), Topographic and ecologic controls on root reinforcement, *J. Geophys. Res.*, *114*, F03013, doi:10.1029/2008JF001168.

Hari, P., A. Makela, F. Berninger, and T. Pohja (1999), Field evidence for the optimality hypothesis of gas exchange in plants, *Aust. J. Plant Physiol.*, *26*, 239–244.

Hari, P., A. Makela, and T. Pohja (2000), Surprising implications of the optimality hypothesis of stomatal regulation gain support in a field test, *Aust. J. Plant Physiol.*, *27*, 77–80.

Hewlett, J. D. (1961), Soil moisture as a source of base flow from steep mountain watersheds, Southeast. For. Exp. Stn., For. Serv., U.S. Dep. of Agric., Asheville, N. C.

Hewlett, J. D., and A. R. Hibbert (1963), Moisture and energy conditions within a sloping soil mass during drainage, *J. Geophys. Res.*, *68*, 1081–1087, doi:10.1029/JZ068i004p01081.

Howes, D. A., and A. D. Abrahams (2003), Modeling runoff and runon in a desert shrubland ecosystem, Jornada Basin, New Mexico, *Geomorphology*, *53*, 45–73, doi:10.1016/S0169-555X(02)00347-1.

Huete, A. R. (1988), A soil-adjusted vegetation index (SAVI), *Remote Sens. Environ.*, *25*, 295–309, doi:10.1016/0034-4257(88)90106-X.

Huete, A., C. Justice, and H. Liu (1994), Development of vegetation and soil indexes for MODIS-EOS, *Remote Sens. Environ.*, *49*, 224–234, doi:10.1016/0034-4257(94)90018-3.

Hui, D. F., and R. B. Jackson (2006), Geographical and interannual variability in biomass partitioning in grassland ecosystems: A synthesis of field data, *New Phytol.*, *169*, 85–93, doi:10.1111/j.1469-8137.2005.01569.x.

Huxman, T. E., et al. (2004), Convergence across biomes to a common rain-use efficiency, *Nature*, *429*, 651–654, doi:10.1038/nature02561.

Ivanov, V. Y., R. L. Bras, and E. R. Vivoni (2008), Vegetation-hydrology dynamics in complex terrain of semiarid areas: 1. A mechanistic approach to modeling dynamic feedbacks, *Water Resour. Res.*, *44*, W03429, doi:10.1029/2006WR005588.

Jackson, R. B., L. A. Moore, W. A. Hoffmann, W. T. Pockman, and C. R. Linder (1999), Ecosystem rooting depth determined with caves and DNA, *Proc. Natl. Acad. Sci. U. S. A.*, *96*, 11,387–11,392, doi:10.1073/pnas.96.20.11387.

Jackson, R. B., et al. (2000), Belowground consequences of vegetation change and their treatment in models, *Ecol. Appl.*, *10*, 470–483, doi:10.1890/1051-0761(2000)010[0470:BCOVCA]2.0.CO;2.

Jarvis, P. G. (1976), The interpretation of the variations in leaf water potential and stomatal conductance found in canopies in the field, *Philos. Trans. R. Soc. London, Ser. B*, *273*, 593–610, doi:10.1098/rstb.1976.0035.

Jobbagy, E. G., and R. B. Jackson (2001), The distribution of soil nutrients with depth: Global patterns and the imprint of plants, *Biogeochemistry*, *53*, 51–77, doi:10.1023/A:1010760720215.

Kerkhoff, A. J., S. N. Martens, and B. T. Milne (2004), An ecological evaluation of Eagleson's optimality hypotheses, *Funct. Ecol.*, *18*, 404–413, doi:10.1111/j.0269-8463.2004.00844.x.

Kim, H. S., R. Oren, and T. M. Hinckley (2008), Actual and potential transpiration and carbon assimilation in an irrigated poplar plantation, *Tree Physiol.*, *28*, 559–577.

Kimball, J. S., P. E. Thornton, M. A. White, and S. W. Running (1997), Simulating forest productivity and surface-atmosphere carbon exchange in the BOREAS study region, *Tree Physiol.*, *17*, 589–599.

Kleidon, A., and M. Heimann (1998), A method of determining rooting depth from a terrestrial biosphere model and its impacts on the global water and carbon cycle, *Global Change Biol.*, *4*, 275–286, doi:10.1046/j.1365-2486.1998.00152.x.

Knoepp, J. D., and W. T. Swank (1998), Rates of nitrogen mineralization across an elevation and vegetation gradient in the southern Appalachians, *Plant Soil*, *204*, 235–241, doi:10.1023/A:1004375412512.

Knoepp, J. D., J. M. Vose, and W. T. Swank (2008), Nitrogen deposition and cycling across an elevation and vegetation gradient in southern Appalachian forests, *Int. J. Environ. Stud.*, *65*, 391–410, doi:10.1080/00207230701862348.

Laio, F., P. D'Odorico, and L. Ridolfi (2006), An analytical model to relate the vertical root distribution to climate and soil properties, *Geophys. Res. Lett.*, *33*, L18401, doi:10.1029/2006GL027331.

Leuning, R. (1995), A critical-appraisal of a combined stomatal-photosynthesis model for C_3 plants, *Plant Cell Environ.*, *18*, 339–355, doi:10.1111/j.1365-3040.1995.tb00370.x.

Litton, C. M., J. W. Raich, and M. G. Ryan (2007), Carbon allocation in forest ecosystems, *Global Change Biol.*, *13*, 2089–2109, doi:10.1111/j.1365-2486.2007.01420.x.

Ludwig, J. A., B. P. Wilcox, D. D. Breshears, D. J. Tongway, and A. C. Imeson (2005), Vegetation patches and runoff-erosion as interacting eco-hydrological processes in semiarid landscapes, *Ecology*, *86*, 288–297, doi:10.1890/03-0569.

Mackay, D. S. (2001), Evaluation of hydrologic equilibrium in a mountainous watershed: Incorporating forest canopy spatial adjustment to soil biogeochemical processes, *Adv. Water Resour.*, *24*, 1211–1227, doi:10.1016/S0309-1708(01)00040-9.

Mackay, D. S., and L. E. Band (1997), Forest ecosystem processes at the watershed scale: Dynamic coupling of distributed hydrology and canopy growth, *Hydrol. Processes*, *11*, 1197–1217, doi:10.1002/(SICI)1099-1085(199707)11:9<1197::AID-HYP552>3.0.CO;2-W.

Martin, J. G., B. D. Kloeppel, T. L. Schaefer, D. L. Kimbler, and S. G. McNulty (1998), Aboveground biomass and nitrogen allocation of ten deciduous southern Appalachian tree species, *Can. J. For. Res.*, *28*, 1648–1659, doi:10.1139/cjfr-28-11-1648.

McConnaughay, K. D. M., and J. S. Coleman (1999), Biomass allocation in plants: Ontogeny or optimality? A test along three resource gradients, *Ecology*, *80*, 2581–2593.

McGinty, D. T. (1976), Comparative root and soil dynamics on a white pine watershed and in the hardwood forest in the Coweeta basin, Ph.D. thesis, Univ. of Ga., Athens.

McMurtrie, R. E., R. Leuning, W. A. Thompson, and A. M. Wheeler (1992), A model of canopy photosynthesis and water use incorporating a mechanistic formulation of leaf CO_2 exchange, *For. Ecol. Manage.*, *52*, 261–278, doi:10.1016/0378-1127(92)90505-4.

Mitchell, K. A., P. V. Bolstad, and J. M. Vose (1999), Interspecific and environmentally induced variation in foliar dark respiration among eighteen southeastern deciduous tree species, *Tree Physiol.*, *19*, 861–870.

Monk, C. D., and F. P. Day (1988), Biomass, primary production, and selected nutrient budgets for an undisturbed watershed, in *Forest Hydrology and Ecology at Coweeta*, edited by W. T. Swank and D. A. Crossley Jr., pp. 151–159, Springer, New York.

Nadelhoffer, K. J., B. A. Emmett, P. Gundersen, O. J. Kjonaas, C. J. Koopmans, P. Schleppi, A. Tietema, and R. F. Wright (1999), Nitrogen deposition makes a minor contribution to carbon sequestration in temperate forests, *Nature*, *398*, 145–148, doi:10.1038/18205.

Nash, J. E., and J. V. Sutcliffe (1970), River flow forecasting through conceptual models part I —A discussion of principles, *J. Hydrol.*, *10*, 282–290, doi:10.1016/0022-1694(70)90255-6.

Nemani, R. R., and S. W. Running (1989), Testing a theoretical climate soil leaf-area hydrologic equilibrium of forests using satellite data and ecosystem simulation, *Agric. For. Meteorol.*, *44*, 245–260, doi:10.1016/0168-1923(89)90020-8.

Nemani, R., L. Pierce, S. Running, and L. Band (1993), Forest ecosystem processes at the watershed scale: Sensitivity to remotely sensed leaf area index estimates, *Int. J. Remote Sens.*, *14*, 2519–2534, doi:10.1080/01431169308904290.

Nepstad, D. C., C. R. Decarvalho, E. A. Davidson, P. H. Jipp, P. A. Lefebvre, G. H. Negreiros, E. D. Dasilva, T. A. Stone, S. E. Trumbore, and S. Vieira (1994), The role of deep roots in the hydrological and carbon cycles of Amazonian forests and pastures, *Nature*, *372*, 666–669, doi:10.1038/372666a0.

Oren, R., and D. E. Pataki (2001), Transpiration in response to variation in microclimate and soil moisture in southeastern deciduous forests, *Oecologia*, *127*, 549–559, doi:10.1007/s004420000622.

Oren, R., et al. (2001), Soil fertility limits carbon sequestration by forest ecosystems in a CO_2-enriched atmosphere, *Nature*, *411*, 469–472, doi:10.1038/35078064.

Parton, W. J., A. R. Mosier, D. S. Ojima, D. W. Valentine, D. S. Schimel, K. Weier, and A. E. Kulmala (1996), Generalized model for N_2 and N_2O production from nitrification and denitrification, *Global Biogeochem. Cycles*, *10*, 401–412, doi:10.1029/96GB01455.

Pierce, L. L., and S. W. Running (1988), Rapid estimation of coniferous forest leaf-area index using a portable integrating radiometer, *Ecology*, *69*, 1762–1767, doi:10.2307/1941154.

Porporato, A., F. Laio, L. Ridolfi, and I. Rodriguez-Iturbe (2001), Plants in water-controlled ecosystems: Active role in hydrologic processes and response to water stress: III. Vegetation water stress, *Adv. Water Resour.*, *24*, 725–744, doi:10.1016/S0309-1708(01)00006-9.

Porporato, A., P. D'Odorico, F. Laio, L. Ridolfi, and I. Rodriguez-Iturbe (2002), Ecohydrology of water-controlled ecosystems, *Adv. Water Resour.*, *25*, 1335–1348, doi:10.1016/S0309-1708(02)00058-1.

Porporato, A., P. D'Odorico, F. Laio, and I. Rodriguez-Iturbe (2003), Hydrologic controls on soil carbon and nitrogen cycles. I. Modeling scheme, *Adv. Water Resour.*, *26*, 45–58, doi:10.1016/S0309-1708(02)00094-5.

Reich, P. B., D. S. Ellsworth, M. B. Walters, J. M. Vose, C. Gresham, J. C. Volin, and W. D. Bowman (1999), Generality of leaf trait relationships: A test across six biomes, *Ecology*, *80*, 1955–1969.

Rodriguez-Iturbe, I., P. D'Odorico, A. Porporato, and L. Ridolfi (1999a), On the spatial and temporal links between vegetation, climate, and soil moisture, *Water Resour. Res.*, *35*, 3709–3722, doi:10.1029/1999WR900255.

Rodriguez-Iturbe, I., P. D'Odorico, A. Porporato, and L. Ridolfi (1999b), Tree-grass coexistence in savannas: The role of spatial dynamics and climate fluctuations, *Geophys. Res. Lett.*, *26*, 247–250, doi:10.1029/1998GL900296.

Running, S. W., and J. C. Coughlan (1988), A general-model of forest ecosystem processes for regional applications. 1. Hydrologic balance, canopy gas exchange and primary production processes, *Ecol. Modell.*, *42*, 125–154, doi:10.1016/0304-3800(88)90112-3.

Running, S. W., and S. T. Gower (1991), FOREST-BGC, a general model of forest ecosystem processes for regional applications. 2. Dynamic carbon allocation and nitrogen budgets, *Tree Physiol.*, *9*, 147–160.

Running, S. W., and E. R. Hunt (1993), Generalization of a forest ecosystem process model for other biomes, BIOME-BCG, and an application for global-scale models, in *Scaling Physiological Processes: Leaf to Globe*, edited by J. R. Ehleringer and C. B. Field, pp. 141–158, Academic, San Diego, Calif.

Running, S. W., R. R. Nemani, and R. D. Hungerford (1987), Extrapolation of synoptic meteorological data in mountainous terrain and its use for simulating forest evapotranspiration and photosynthesis, *Can. J. For. Res.*, *17*, 472–483, doi:10.1139/x87-081.

Ryan, M. G. (1991), Effects of climate change on plant respiration, *Ecol. Appl.*, *1*, 157–167, doi:10.2307/1941808.

Ryan, M. G., D. Binkley, J. H. Fownes, C. P. Giardina, and R. S. Senock (2004), An experimental test of the causes of forest growth decline with stand age, *Ecol. Monogr.*, *74*, 393–414, doi:10.1890/03-4037.

Saco, P. M., G. R. Willgoose, and G. R. Hancock (2007), Eco-geomorphology of banded vegetation patterns in arid and semi-arid regions, *Hydrol. Earth Syst. Sci.*, *11*, 1717–1730.

Schenk, H. J., and R. B. Jackson (2002), Rooting depths, lateral root spreads and below-ground/above-ground allometries of plants in water-limited ecosystems, *J. Ecol.*, *90*, 480–494, doi:10.1046/j.1365-2745.2002.00682.x.

Schenk, H. J., and R. B. Jackson (2005), Mapping the global distribution of deep roots in relation to climate and soil characteristics, *Geoderma*, *126*, 129–140, doi:10.1016/j.geoderma.2004.11.018.

Schimel, D. S., B. H. Braswell, and W. J. Parton (1997), Equilibration of the terrestrial water, nitrogen, and carbon cycles, *Proc. Natl. Acad. Sci. U. S. A.*, *94*, 8280–8283, doi:10.1073/pnas.94.16.8280.

Schymanski, S. J., M. L. Roderick, M. Sivapalan, L. B. Hutley, and J. Beringer (2008a), A canopy-scale test of the optimal water-use hypothesis, *Plant Cell Environ.*, *31*, 97–111, doi:10.1111/j.1365-3040.2007.01740.x.

Schymanski, S. J., M. Sivapalan, M. L. Roderick, J. Beringer, and L. B. Hutley (2008b), An optimality-based model of the coupled soil moisture and root dynamics, *Hydrol. Earth Syst. Sci.*, *12*, 913–932.

Sellers, P. J., J. A. Berry, G. J. Collatz, C. B. Field, and F. G. Hall (1992), Canopy reflectance, photosynthesis, and transpiration. 3. A reanalysis using improved leaf models and a new canopy integration scheme, *Remote Sens. Environ.*, *42*, 187–216, doi:10.1016/0034-4257(92)90102-P.

Sullivan, N. H., P. V. Bolstad, and J. M. Vose (1996), Estimates of net photosynthetic parameters for twelve tree species in mature forests of the southern Appalachians, *Tree Physiol.*, *16*, 397–406.

Swift, L. W. J., G. B. Cunningham, and J. E. Douglass (1988), Climatology and hydrology, in *Forest Hydrology and Ecology at Coweeta*, edited by W. T. Swank and D. A. Crossley, Jr., pp. 35–55, Springer, New York.

Tague, C. L., and L. E. Band (2004), RHESSys: Regional Hydro-Ecologic Simulation System—An object-oriented approach to spatially distributed modeling of carbon, water, and nutrient cycling, *Earth Interact.*, *8*, 1–42, doi:10.1175/1087-3562(2004)8<1:RRHSSO>2.0.CO;2.

Taiz, L., and E. Zeiger (2002), *Plant Physiology*, 3rd ed., Sinauer, Sunderland, Mass.

Tarboton, D. G. (1997), A new method for the determination of flow directions and upslope areas in grid digital elevation models, *Water Resour. Res.*, *33*, 309–319, doi:10.1029/96WR03137.

Thornton, P. E. (1998), Regional ecosystem simulation: Combining surface- and satellite-based observations to study linkages between terrestrial energy and mass budgets, Ph.D. thesis, Univ. of Mont., Missoula.

Thornton, P. E., et al. (2002), Modeling and measuring the effects of disturbance history and climate on carbon and water budgets in evergreen needleleaf forests, *Agric. For. Meteorol.*, *113*, 185–222, doi:10.1016/S0168-1923(02)00108-9.

Tilman, D. (1988), *Plant Strategies and the Dynamics and Structure of Plant Communities*, Princeton Univ. Press, Princeton, N. J.

Todd, R. L., J. B. Waide, and B. W. Cornaby (1975), Significance of biological nitrogen fixation and denitrification in a deciduous forest ecosystem, in *Mineral Cycling in Southeastern Ecosystems*, edited by F. G. Howell, J. B. Gentry, and M. H. Smith, pp. 729–735, Tech. Inf. Cent., Off. of Public Affairs, U.S. Energy Res. and Dev. Admin., Oak Ridge, Tenn.

van der Tol, C., A. G. C. A. Meesters, A. J. Dolman, and M. J. Waterloo (2008a), Optimum vegetation characteristics, assimilation, and transpiration during a dry season: 1. Model description, *Water Resour. Res.*, *44*, W03421, doi:10.1029/2007WR006241.

van der Tol, C., A. J. Dolman, M. J. Waterloo, and A. G. C. A. Meesters (2008b), Optimum vegetation characteristics, assimilation, and transpiration during a dry season: 2. Model evaluation, *Water Resour. Res.*, *44*, W03422, doi:10.1029/2007WR006243.

Vitousek, P. M., and R. W. Howarth (1991), Nitrogen limitation on land and in the sea—How can it occur?, *Biogeochemistry*, *13*, 87–115, doi:10.1007/BF00002772.

Vose, J. M., and P. V. Bolstad (1999), Challenges to modelling NPP in diverse eastern deciduous forests: Species-level comparisons of foliar respiration responses to temperature and nitrogen, *Ecol. Modell.*, *122*, 165–174, doi:10.1016/S0304-3800(99)00136-2.

Vose, J. M., and P. V. Bolstad (2007), Biotic and abiotic factors regulating forest floor CO_2 flux across a range of forest age classes in the southern Appalachians, *Pedobiologia*, *50*, 577–587, doi:10.1016/j.pedobi.2006.10.006.

Wang, Y. P., and R. Leuning (1998), A two-leaf model for canopy conductance, photosynthesis and partitioning of available energy I: Model description and comparison with a multi-layered model, *Agric. For. Meteorol.*, *91*, 89–111, doi:10.1016/S0168-1923(98)00061-6.

White, M. A., P. E. Thornton, S. W. Running, and R. R. Nemani (2000), Parameterization and sensitivity analysis of the BIOME-BGC terrestrial ecosystem model: Net primary production controls, *Earth Interact.*, *4*, 1–85, doi:10.1175/1087-3562(2000)004<0003:PASAOT>2.0.CO;2.

Whittaker, R. H. (1956), Vegetation of the Great Smoky Mountains, *Ecol. Monogr.*, *26*, 1–69, doi:10.2307/1943577.

Wigmosta, M. S., L. W. Vail, and D. P. Lettenmaier (1994), A distributed hydrology-vegetation model for complex terrain, *Water Resour. Res.*, *30*, 1665–1679, doi:10.1029/94WR00436.

Wilson, J. B. (1988), A review of evidence on the control of shoot-root ratio, in relation to models, *Ann. Bot.*, *61*, 433–449.

Wilson, K. B., D. D. Baldocchi, and P. J. Hanson (2000), Spatial and seasonal variability of photosynthetic parameters and their relationship to leaf nitrogen in a deciduous forest, *Tree Physiol.*, *20*, 565–578.

Wilson, K. B., P. J. Hanson, P. J. Mulholland, D. D. Baldocchi, and S. D. Wullschleger (2001), A comparison of methods for determining forest evapotranspiration and its components: Sap-flow, soil water budget, eddy covariance and catchment water balance, *Agric. For. Meteorol.*, *106*, 153–168, doi:10.1016/S0168-1923(00)00199-4.

Wullschleger, S. D. (1993), Biochemical limitations to carbon assimilation in C_3 plants—A retrospective analysis of the A/C_i curves from 109 species, *J. Exp. Bot.*, *44*, 907–920, doi:10.1093/jxb/44.5.907.

Yeakley, J. A., W. T. Swank, L. W. Swift, G. M. Hornberger, and H. H. Shugart (1998), Soil moisture gradients and controls on a southern Appalachian hillslope from drought through recharge, *Hydrol. Earth Syst. Sci.*, *2*, 41–49.

Zak, D. R., D. Tilman, R. R. Parmenter, C. W. Rice, F. M. Fisher, J. Vose, D. Milchunas, and C. W. Martin (1994), Plant production and soil microorganisms in late-successional ecosystems—A continental-scale study, *Ecology*, *75*, 2333–2347, doi:10.2307/1940888.

L. Band and T. Hwang, Department of Geography and Institute for the Environment, University of North Carolina at Chapel Hill, Chapel Hill, NC 27599, USA. (h7666@email.unc.edu)

T. C. Hales, School of Earth and Ocean Sciences, Cardiff University, Cardiff CF11 9NY, UK.